Composites as Enabling Technology in Flow Assurance

By

© Samar Aly

A dissertation submitted to the School of Graduate Studies

in partial fulfillment of the requirements for the degree of

Master of Mechanical Engineering

Faculty of Engineering and Applied Science

Memorial University of Newfoundland

August 2020

St. John’s, Newfoundland, Canada

Abstract

In oil and gas production, flow assurance guarantees a successful and economical flow of the fluids from the reservoir to a designated processing facility. Flow assurance is one of the biggest challenges that a pipeline designer faces, especially under deep water where the temperature is low, and the pressure is high. These deep-water conditions favor the formation of solid deposits, which leads to blocking the flow line, reducing oil production, and potentially shutting down the well. To avoid this problem, the flow line temperature must always be kept above the solid deposit formation temperature. This necessitates accurate analysis of the thermal properties of pipelines in order to choose the best material suitable under these harsh conditions.

This thesis provides a quantitative comparison based on thermal characteristics for flow assurance purposes. It also provides a realistic comparison based on strength requirement imposed on risers in general. First, we present a comparison between two different solutions (analytical and approximate) to predict the temperature profile in the steady state flow case. This comparison is carried on a steel pipeline under different cases, which are obtained by varying the length of the pipeline and the flow rate.

Based on the results of the comparison, the solution that meets the objectives of this thesis is identified.

Then, the thesis focuses on the effect of using different materials in the pipeline. The thesis presents another comparison between traditional steel catenary risers (SCR) and Composite

Catenary Risers (CCR) based on their thermal characteristics for flow assurance purposes. The comparison is based on predicting the fluid flow temperature along the pipeline to show which material will keep the temperature above the solid deposit formation temperature, which is set in this thesis to be 20℃. Nominal homogenized mechanical and heat transfer properties are used for composite and steel pipelines of the same thickness and diameter. The obtained results show that composite risers have enhanced thermal characteristics over its counterpart steel pipelines. To establish rational comparisons between SCR and CCR, other aspects of their performance must be considered. Performance aspects regarding material strength, expected life and minimal weight design constitute the most essential minimal set for these comparisons. Comprehensive investigations are conducted, and conclusions are extracted to quantify overall performance aspects of SCR and CCR. All the code used to run the experiments was implemented in MATLAB.

To my family for all the support throughout the years….

And to my supervisor, Dr. Nakhla, who believed in me and encouraged me a lot, I really appreciate his support, motivation, encouragement, his valuable comments and his valuable time

COVID-19 Statement

COVID-19 has changed many aspects of how I live my life. As a mother, one of the biggest adjustments I have had to make is having all of my kids stay at home. My two youngest boys are 10 and 16. They made the change to online school very suddenly, so we have all had to adjust. They have had to use my laptop for online zoom meetings, as well as when they are doing their homework, so I have not had the same amount of access to my laptop as I normally would. This made it increasingly difficult to work on my thesis. Additionally, living with my mother-in-law (75 years old) and my diabetic husband has made us take extra precautions with all of our activities, including the simple grocery shopping. Buying groceries takes almost twice as long now, because we unpack all of the groceries before entering the house and wash them to ensure my mother-in-law's safety. Although we have privileges like access to the internet, food, and secure housing, COVID-19 has presented me with other challenges that I did not expect to face.

Table of Contents

List of Figures

List of Tables

Nomenclature

A_i Area of pipeline inner surface (m^2)

A_o Area of pipeline outer surface (m^2)

A_r Area of pipeline at the reference radius (m^2)

B Constant of integration

C Constant of integration

C_p Specific heat of fluid at constant pressure ($J/kg\ °C$)

f Arbitrary function

G Thermal gradient outside the insulation ($°C/m$)

h_i Film coefficient of pipeline inner surface

h_o Film coefficient of pipeline outer surface

k Thermal conductivity of insulation layer($W/m\ °C$)

K Characteristic variable

k_m Thermal conductivity of layer m $(W/m\ °C)$

L Longitudinal distance from the fluid entry point (m)

m Layer index

q Rate of heat transfer over the whole length of pipe caused by radial conduction (W)

q_{acc} Heat accumulation (J)

q_{in} Heat flow in (J)

q_{out} Heat flow out (J)

q_r Heat transferred (J)

Q_R Heat-transfer rate (W)

r Radial distance (m)

R Inner radius of insulation layer (m)

r_m Radius of layer m (m)

s Thickness of insulation layer (m)

T Temperature inside the pipe $(°C)$

T_o Temperature of outer medium at the fluid entry point $(°C)$

T_L Temperature of flowing-in fluid $(°C)$

$T_{L+\Delta L}$ Temperature of flowing-out fluid $(°C)$

T_s Temperature of fluid at the fluid entry point ($°C$)

u Variable

U Overall heat transfer coefficient (OHTC) $(W/m^2 - °C)$

v The average flow velocity of fluid in the pipe $(\frac{m}{s})$

$\alpha, \beta \; and \; \gamma$ Variables

ΔL Length of pipe segment (m)

Δt Time period (s)

ΔT Different in temperature between pipeline product and the ambient temperature outside $(°C)$

θ Angle between the principle thermal gradient and pipe orientation $degrees$

ρ Fluid density (kg/m^3)

t Time $seconds$

$\dot{m}$ Mass flow rate of internal flow fluid (kg/s)

u The displacement at any point in the x-direction (m)

v The displacement at any point in the y-direction (m)

ε_x The strains in the x-direction

ε_y The strains in the y-direction

γ_{xy} The shear strain

$\varepsilon^o{}_x$ The midplane normal strain in the x-direction

$\varepsilon^o{}_y$ The midplane normal strain in the y-direction

$\gamma^o{}_{xy}$ The midplane shear strain

κ_x The midplane bending curvature in the x-direction

κ_y The midplane bending curvature in the y-direction

κ_{xy} The midplane twisting curvature

σ_x The normal stress in the x-direction (Pa)

σ_y The normal stress in the y-direction (Pa)

τ_{xy} The shear stress (Pa)

$[\bar{Q}]$ The stiffness matrix for the laminate (Pa)

N_x Normal force resultant in the x-direction per unit width(N/m)

N_y Normal force resultant in the y-direction per unit width (N/m)

N_{xy} Shear force resultant in the y-direction per unit width (N/m)

M_x Bending moment resultant in the yz-plane per unit width (N)

M_y Bending moment resultant in the xz-plane per unit width (N)

M_{xy} Twisting moment resultant per unit width (N)

$[A]$ Extensional stiffness matrix for the laminate (N/m)

$[B]$ Coupling stiffness matrix for the laminate (N)

$[D]$ Bending stiffness matrix for the laminate $(N.m)$

E_{xx} The longitudinal Young Modulus (Pa)

ν_{xy} The Major Poisson Ratio

G_{xy} The Shear Modulus (Pa)

σ The normal stress (Pa)

F The axial force (N)

M Moment of neutral axis $(N.m)$

y The perpendicular distance to the neutral axis (m)

I The second moment of area (m^4)

P_E Buckling Load (N)

W_p The pipe weight per unit length (N/m)

γ The specific weight (N/m^3)

P Pipeline design pressure (bar)

Chapter 1 : Introduction and Overview

1.1 Overview

Pipelines are an essential aspect of any oil and gas production system. They are used to transfer the liquid or gas between the production site and the reception site. A pipeline system is defined as a pipeline section extending from an inlet point to an outlet point [1]. Figure 1-1 shows pipelines in an underwater environment.

Figure 1-1: Underwater pipelines, photo courtesy of [2]

Flow assurance is one of the biggest challenges that a pipeline designer faces, particularly with pipelines under deep water, where temperatures are very low, and the pressure is high. These conditions favor the formation of solid deposits, which can lead to the following consequences: blockage of the flowline, reduction in oil production, and potentially causing the shutdown of the well. The most important components of solid deposits include hydrate, paraffin wax, and asphaltene [3].

Hydrate deposits, as shown in Figure 1-2, are created due to the contact between water molecules and hydrocarbon molecules under low temperature and high-pressure conditions. When water molecules are formed around individual gas molecules, hydrate crystals are formed, which will have a similar shape, and physical and mechanical properties as ice [4]. However, it is important to note that hydrate crystals are not ice. Under low temperature and high-pressure conditions, the dissolved wax in the oil starts to switch from a liquid state into a solid state. The wax crystals start to form when the crude temperature drops under a certain temperature. This is called the cloud point. The asphaltene solids are sticky black coal with a density of around 1.3 g/cm^3, and they are difficult to remove [4].

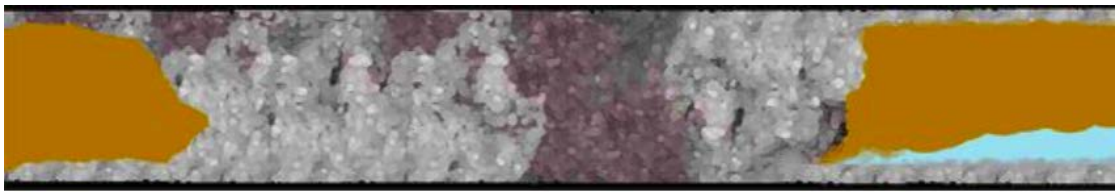

Figure 1-2: Hydrate formation, photo courtesy of [5]

The designers have to investigate and balance many parameters to prevent the formation of deposits and guarantee flow assurance, including: 1) Pipeline material (steel, composite, alloy, etc.), 2) Diameter of the pipeline, 3) Wall thickness of pipeline, 4) Pipeline length, 5) Internal and external pressure, 6) Flow rate, and 7) Ambient and operating temperature.

There are many methods that can be used to avoid (or minimize) the solid deposit formation problem and hence guarantee flow assurance. These methods can broadly be categorized as follows: 1) Chemical-based methods, 2) Mechanical-based methods, and 3) Thermal design-based methods.

For chemical-based methods, the designers use [6]:

1- Thermodynamic inhibitors (such as methanol, glycol, etc.) are injected in order to prevent the formation of deposits. They are used to reduce the hydrate formation temperature. This is considered the most common solution.
2- Low-dosage hydrate inhibitors (LDHIs). These use a dynamic inhibitor to defer the hydrate formation.
3- Water removal, which uses the dehydration technique through the flowline.

For mechanical-based methods the designers use [7]:

1- Depressurization, where the line slowly depressurizes from both sides of the plug [6].
2- Pigging, which is a process that pushes the hydrate out of the pipe by running a pig with a smaller diameter plate inside the pipeline to clean all the deposits.

For thermal design-based methods, the designers use [8]:

1- Thermal insulation, which is one of the most important methods to avoid gas hydrate and wax formation. With this method, the designer uses different insulation materials (such as polypropylene, polyurethane, epoxy, etc.) as an external coating for the pipeline to prevent any decrease in the flow oil temperature.
2- Active heating, which uses electrical heating or hot fluid circulation to keep the flowline above the deposit formation temperature.
3- Pipe in pipe (PIP). In this method, an inner insulating pipe is responsible for carrying the flow oil and another external pipe works as a sleeve for the inner pipe. This setup

helps to keep the temperature above the required threshold, and hence minimizes deposits formation.

This thesis focus on the thermal design-based methods but from a new perspective. The use of thermal design methods has been studied extensively in literature. Many studies focus on pipeline insulation using different insulation materials with different thicknesses, to keep the crude temperature above the design requirement; for example, the study of [6]. In other studies, they focus on a special heating system (hot fluid or electrical heating) around the pipeline or PIP (pipe in pipe) or HPIP (heated pipe in pipe); for example, the study of [9].

Overall, based on the literature review, the pipeline's designers must consider three aspects simultaneously to generate an efficient and effective design; these are:

1) The structural aspect of the pipeline design (e.g., diameter and thickness of the pipeline).
2) The flow assurance aspect, which prevents the formation of deposits.
3) The economic aspect, which includes the cost of the design (e.g., the material being used, steel vs. composite, and the maintenance cost in the long run).

1.2 **Thesis Scope**

In this thesis, the focus is on guaranteeing flow assurance (point number 2 above) using thermal design-based methods. We also focus on the pipeline material itself (points number 2 and 3 above) to make sure that the temperature at any point in the pipeline is always above the solid deposit formation temperature, while still in a feasibly economical manner. The proper selection of the pipeline material and its design parameters, such as the

diameter and the thickness (point 1 above), will prevent many of the problems discussed in the previous section.

1.3 Thesis Contribution

There is a lack of full quantitative studies covering all aspects of comparison between traditional steel and composite risers in the under deep-water condition. This thesis provides a realistic comparison based on thermal characteristics, mechanical characteristics (e.g., weight, failure, bending, buckling, strength, and corrosion), and economical characteristics (e.g., cost).

The main contribution of this research can be summarized as follows:

- A study and implementation to compare two models **to predict the temperature profile in the steady state flow based** on: 1) An analytical solution, and 2) An approximate solution. The implementation is done using Matlab.
- A comparison between the two prediction models on traditional steel pipelines.
- Selection of the best suitable model and using it to compare the temperature profiles of steel pipelines and composite pipelines.
- A comparison of the steel and composite pipelines in terms of other design parameters (such as weight, bending, strength, corrosion, and cost).

1.4 **Publications**

The work presented in this thesis was accepted and published in:

- Samar Aly, Samer Nakhla, “Thermal Characteristics of Steel and Composite Risers for Flow Assurance”, Proceedings of The Joint Canadian Society for Mechanical Engineering and CFD Society of Canada International Congress 2019, June 2-5, 2019, London, On, Canada

1.5 **Thesis Outline**

The remainder of the thesis is organized as follows. Chapter 2 presents the two prediction models for the pipeline temperature profile. Chapter 3 discusses the mechanical properties and the design considerations for composite pipelines. Chapter 4 presents the thesis conclusions and recommendations.

Chapter 2 : Thermal Characteristics

2.1 Overview

Flow assurance, pipeline material, thickness, diameter and the working temperature and pressure are considered critical aspects that pipeline designers must consider in order to generate an efficient and effective design. For example, the term flow assurance was first used by Petrobras in the early 1990s in Portuguese as *"Garantia do Escoamento"*, meaning literally *"Guarantee of Flow"*, or Flow Assurance [10].

Flow assurance can be affected by the presence of solid deposits, which form when the temperature of the hydrocarbon flow drops below the formation temperature. Figure 2-1 shows natural gas hydrate formation as a function of temperature and pressure. The curve shows two main regions. The right of the curve is the hydrates free region (no hydrates formation in this zone); this area on the right is the safe operation area. The left region of the curve is where the formation of hydrates is most likely to occur.

To avoid this problem, the flow line temperature must always be kept above the solid deposit formation temperature. This necessitates accurate predictions of the internal pipeline temperature to make sure that the temperature at any point is always above the solid deposit formation temperature.

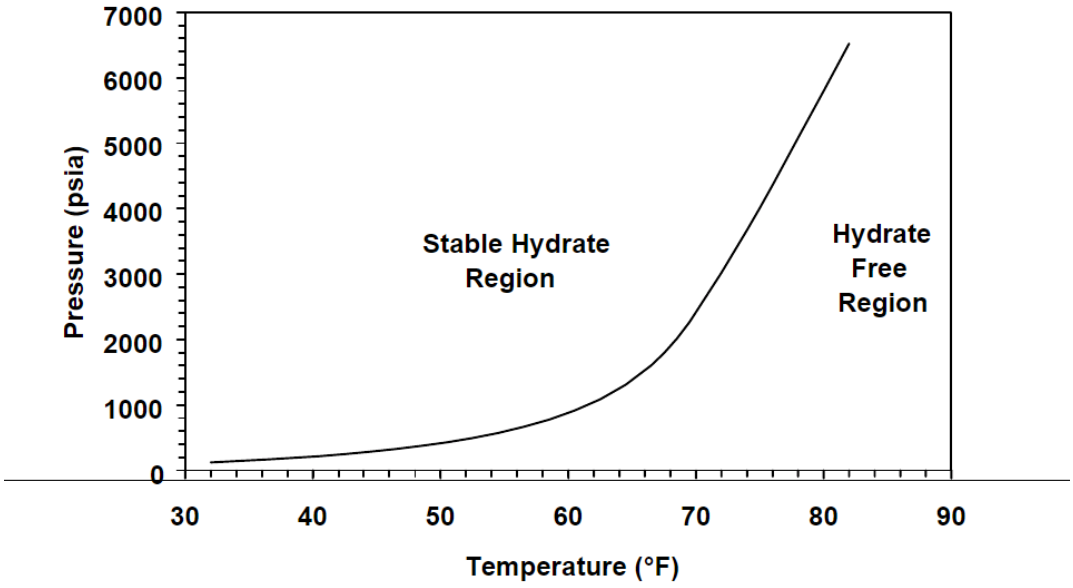

Figure 2-1: The Hydrate Formation curve, figure courtesy of [4]

The main objective of this chapter is to investigate the thermal characteristics in pipelines to guarantee that the fluid flow temperature will remain above the deposit and solid formation temperature. This can be achieved by accurately predicting the fluid temperature along the pipeline length and calculating the heat loss along the pipeline.

2.2 Literature Review

According to Kirkpatrick [11] it is essential to apply temperature calculating techniques before the pipeline installation. Many models were developed to predict the heat transfer, and hence the temperature profile on wellbore during oil production. Ramey [12] proposed an equation to predict the fluid temperature in injection wells. He derived a mathematical heat-transfer for an outer medium that is infinitely large.

Later, Willhite [13] presented a mathematical model to calculate the overall heat transfer coefficients (OHTC). He also presented a method to prevent casing failure due to thermal stress in hot water injection.

Other studies were conducted between 1994-2002 by Hasan, Kabir, and Wang [14, 15]. Their studies were also focused on calculating wellbore heat transfer.

More recently, Guo et al. [16] presented a simple model for predicting heat loss and temperature profiles in insulated pipelines. In their work, three analytical heat transfer solutions were presented to predict the heat loss and temperature profiles, one for the steady state flow and the other two are for the transient state flow. Guo et al. considered three different insulation materials (polyethylene, polypropylene and polyurethane) with different thicknesses, and used their proposed mathematical model to find the best type of insulation and thickness. Their model assumed a single insulation layer material with a specific thickness to meet a prerequisite design temperature at any point inside the pipeline.

Although the proposed model showed good results, this work in [17] assumed:

1- Negligible heat transfer via conduction in the longitudinal direction.
2- Negligible variation in temperature as function of radius.
3- Negligible heat due to fraction.
4- Very low thermal conductivity of the insulation material compared to the pipeline.
5- Linear outer temperature in the longitudinal direction.
6- Constant fluid heat capacities.
7- Negligible heat capacities of the pipe and its insulation.

The model presented in [17] assumed normal operating conditions for oil wells and pipelines transporting liquids in order for the above assumptions to be valid.

Further drawbacks of the model presented in [17] are identified by the results of this thesis:

1) The model did not take into account the material of the internal pipeline itself, although it may have a significant impact on the temperature profile.
2) The model did not address the situation of multi-layer insulation.
3) The model was only tested on short pipelines with lengths not exceeding 8047 meters. This was proven to be a serious drawback, which will be discussed later in this chapter.

Su et al. presented in [9] a framework for the thermal design of multi-layered composite pipelines for deep water oil and gas production. They presented two solutions one for steady state flow and another for transient heat transfer analysis. Su et al. also presented a numerical example with a dataset and used a lower thermal conductivity polypropylene foam as insulation. The results show that the polypropylene foam improved the temperature profile. The work of Sue et al. used a one dimensional energy equation that was originally presented in Bai et al. [6] for the steady state flow case while they used a second order accurate explicit finite difference scheme that was initially developed by Warming and Beam [18] in the transient state flow case.

The work of Sue et al. was based on the following assumptions (for more details, refer to [9]):

1) The mass flow rate is constant.

2) The OHTC (U) is constant.

3) The outer temperature is constant.

4) The fluid properties are constant throughout the pipeline.

5) No heat generation in the medium.

6) The pipeline consists of multilayered homogeneous, isotropic materials.

Based on the above, it is obvious that there are two sets of solutions with specific assumptions that were not fully tested under different datasets and with different pipeline lengths. This chapter presents a comparison between the following two models in the steady state flow case: 1) An approximate solution [16] and 2) An exact equation for energy conservation for fluid transport in pipelines [6]. Therefore, these two models are tested on two base datasets of pipelines. The comparison between the two models can help designers to choose the best solution depending on the available data to make a quick estimation for the internal temperature distribution along the pipelines before using other complicated computer programs.

2.3 Temperature Prediction Solutions: Approximate versus Analytical

Many complex computer algorithms can predict the internal pipeline temperature. However, these programs are computationally expensive, and their accuracy can be degraded if larger segmentation is used in long pipelines.

To avoid the formation of solid deposits, the internal temperature must be kept by design above a certain value that is determined by flow assurance criteria. Different solutions have been proposed to guarantee continuous flow; one of the most effective solutions being to choose a pipeline's material which has very low thermal conductivitiy.

Under deep-water, the fluid flow temperature drops inside the pipeline due to convective heat transfer from fluid flow to the inside layer of the pipeline, conductive heat transfer through the pipeline layers, and convective heat transfer from the outer layer of the pipeline to the surrounding fluid. There is also radiative heat transfer from the pipeline to the surroundings. However, this radiative heat transfer is negligible compared to the other forms of heat transfer.

2.3.1 An Approximate Solution (GUO et al. [16])

All the equations and derivations in this subsection are reproduced from Guo et al. [16]. Three analytical heat transfer solutions were proposed in this work to predict heat loss and temperature profiles in pipelines, one for the steady state flow and the other two are for the transient state flow.

A pipeline operates under steady state operation for the majority of operation time. Meanwhile, transient operation dominates instances of production interruption. Therefore,

this thesis focuses only on the internal temperature profile under steady state flow, hence the work of Guo et al. is presented in the steady state flow only. Guo et al. calculate the temperate T inside the pipeline at longitudinal length L using the following mathematical model:

$$T = \frac{1}{\alpha^2}\left(\beta - \alpha\beta L - \alpha\gamma - e^{-\alpha(L+C.)}\right) \tag{2.1}$$

Where:

$$\alpha = \frac{2\pi Rk}{\upsilon\rho C_p sA}$$

$$\beta = \alpha G cos(\Theta)$$

$$\gamma = -\alpha T_0$$

$$C = -\frac{1}{\alpha}\ln(\beta - \alpha^2 T_s - \alpha\,\gamma)$$

Where T_0 is the ambient temperature of the pipe surroundings at $L = 0$, G is the thermal gradient in the external medium, θ is the angle between the thermal gradient and the pipe axis, s is the thickness of the insulation layer, ρ is the fluid density, C_p is the specific heat at constant pressure, υ is the average velocity of fluid in the pipe, A is the cross sectional area of the pipeline, R is inner radius of insulation layer, and k is thermal conductivity of the insulation layer.

Guo et al. used different types of insulation material that are shown in Table 2.1. They also changed the insulation material thickness in order to guarantee that at any point in the pipelines the temperature will never drop below $25°C$, a temperature required by the flow

assurance table. The reported results showed that either a polyurethane layer of thickness 1.5 in (0.0381 m) or a polypropylene layer of thickness 2 in (0.0508 m) will maintain a temperature above 25°C in the pipeline of a length 8047 m.

Table 2.1: Guo et al. material properties

Thermal conductivity for different insulation material	
Material	Thermal conductivity $W/m-$℃
Polyethylene	0.35
Polypropylene	0.22
Polyurethane	0.12

Derivation of the approximate solution (Guo et al.):

The derivation presented in this subsection is reproduced from [9] and represented here for convenience and better understanding of the model.

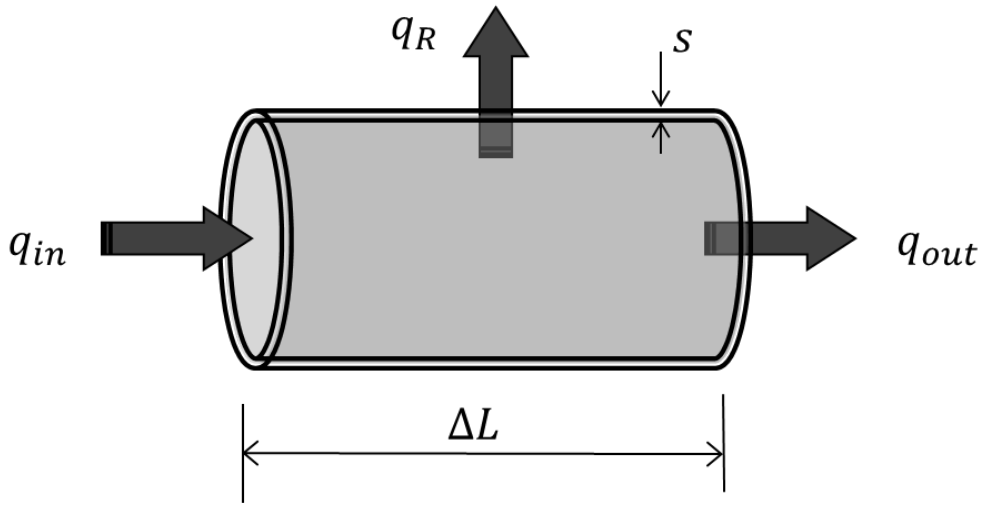

Figure 2-2: Heat flow in a section of a pipeline, figure courtesy of [16]

The heat balance equation

$$q_{in} - q_{out} - q_R = q_{acc} \tag{2.2}$$

Where q_{in} is the heat flow in, q_{out} is the heat flow out, q_r is the heat transferred and q_{acc} is the heat accumulation.

$$q_{in} = \rho C_p \upsilon A T_L \Delta t \tag{2.3}$$

Where ρ is the fluid density, C_p is the specific heat at constant pressure, υ is the average velocity of fluid in the pipe, A is the cross sectional area of the pipeline, T_L is temperature of the flowing-in fluid and Δt is the time period.

$$q_{out} = \rho C_p \upsilon A T_{L+\Delta L} \Delta t \tag{2.4}$$

Where $T_{L+\Delta L}$ is temperature of the flowing-out fluid.

$$q_R = 2\pi R k \Delta L \left(\frac{\partial T}{\partial r}\right) \Delta t \tag{2.5}$$

Where R is inner radius of the insulation layer, k is thermal conductivity of the insulation layer, ΔL is length of the pipe segment and $\frac{\partial T}{\partial r}$ is the radial temperature gradient in the insulation layer.

$$q_{acc} = \rho C_p A \Delta L \Delta \bar{T} \tag{2.6}$$

Where $\Delta \bar{T}$ is the average temperature increase in the pipe segment, and L is the longitudinal distance from the fluid entry point.

Substituting Equations 2.3, 2.4, 2.5, 2.6 into Equation 2.2, and dividing the equation by $\Delta L \Delta t$ results in

$$\rho C_p v A \left(\frac{T_L - T_{L+\Delta L}}{\Delta L}\right) - 2\pi R \left(k \frac{\partial T}{\partial r}\right) = \rho C_p A \frac{\Delta \bar{T}}{\Delta t}$$

Dividing the above equation by $\rho C_p A$ and for the infinitesimal of ΔL and Δt results in

$$v \frac{\partial T}{\partial L} + \frac{\partial T}{\partial t} = -\frac{2\pi R k}{\rho C_p A} \frac{\partial T}{\partial r} \tag{2.7}$$

Where $\frac{\partial T}{\partial r}$ is the radial temperature gradient which can be can expressed as:

$$\frac{\partial T}{\partial r} = \frac{(T - (T_0 - G cos(\theta) L))}{s} \tag{2.8}$$

Where T_0 is the ambient temperature of the pipe surroundings at $L = 0$, G is the thermal gradient in the external medium, θ is the angle between the thermal gradient and the pipe axis, and s is the thickness of the insulation layer.

Substituting Equation 2.8 into Equation 2.7 gives:

$$v \frac{\partial T}{\partial L} + \frac{\partial T}{\partial t} = aT + bL + c \tag{2.9}$$

Where the constants a, b and c are expressed as

$$a = -\frac{2\pi R k}{\rho C_p A s} \tag{2.9.1}$$

$$b = a\, G cos(\theta) \tag{2.9.2}$$

$$c = -aT_0 \tag{2.9.3}$$

And with boundary conditions of

$$T = T_s \; at \; L = 0$$

Dividing all terms in Equations 2.9 by the average velocity v, and applying the above boundary conditions gives

$$\frac{dT}{dL} + \alpha T + \beta L + \gamma = 0 \tag{2.10}$$

Where $\alpha = -{}^{a}/_{v}$, $\beta = -{}^{b}/_{v}$ and $\gamma = -{}^{c}/_{v}$

Assume $$u = \alpha T + \beta L + \gamma \tag{2.11}$$

Then $$T = \frac{u-\beta L-\gamma}{\alpha} \tag{2.12}$$

And $$\frac{dT}{dL} = \frac{1}{\alpha}\frac{du}{dL} - \frac{\beta}{\alpha} \tag{2.13}$$

Substituting Equations 2.12 and 2.13 into 2.10 and integrating the outcome equation with the method of separation of variables yields

$$-\frac{1}{\alpha}\ln(\beta - \alpha u) = L + C \tag{2.14}$$

Substituting u from Equation 2.11 into Equation 2.14 to verify Equation 2.1 gives

$$T = \frac{1}{\alpha^2}(\beta - \alpha\beta L - \alpha\gamma - e^{-\alpha(L+C)})$$

Where the constant of integration, C, is

$$C = -\frac{1}{\alpha}\ln(\beta - \alpha^2 T_s - \alpha\gamma)$$

2.3.2 An Analytical Solution (Bai et al. [6])

Bai et al. presented in [6] a model to calculate the temperature of the fluid at any point along a pipeline. The model was based on the energy conservation between the heat transfer rate through pipe wall and the fluid thermal energy change. All the equations and derivations in this subsection are taken from [6] and [9].

The analytical solution model used the following equation

$$T(x) = T_o + (T_{in} - T_o)\exp(-\frac{U\pi Dx}{\dot{m}c_p}) \quad (2.15)$$

Where $T(x)$ is the temperature of the fluid at distance x from the inlet, T_{in} is the inlet temperature of fluid, $\dot{m}$ is the mass flow rate of the internal fluid, c_p is the specific heat of the internal fluid, U is the overall heat transfer coefficient (OHTC), D is the diameter, T_o is the ambient temperature of the pipe surrounding. The material that was used in the experiment by Bai et al. are listed in Table 2.2. The results show that the best insulation is achieved using polypropylene.

Table 2.2: Datasets used in Bai et al.

Pipeline outer Diameter D_O	0.219 m
Pipeline wall thickness t	0.0143 m
Fluid Density ρ	795.8 kg/m^3
Fluid specific heat C_p	3054 Jkg^{-1}℃
Entry Fluid Temperature T_s	87℃
Ambient Temperature T_O	4℃

Derivation of (1D) analytical solution:

The derivation presented in this subsection is taken from [6] and represented here for complete understanding of the model.

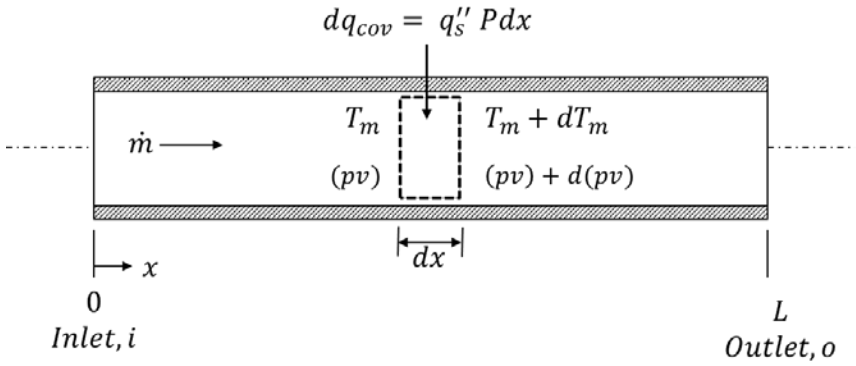

Figure 2-3: Heat flow in a section of a pipeline, figure courtesy of [6]

In subsea pipeline thermal design, there are three modes of heat transfer, namely: conduction, convection, and radiation. Convection will occur between fluid flow in the pipeline and the internal pipeline layer and will also occur between the external pipeline layer and the surrounding fluid due to the temperature difference between the pipeline and the fluid. Conduction will occur due to the temperature difference between the pipeline layers itself. Radiation will occur due to the solid surface temperature. However, since the radiative heat transfer is a small amount compared to the convection and the conduction heat transfer amounts, it will be ignored.

To predict an analytical solution for the temperature profile along the pipeline length, the solution assumes an average velocity of the produced fluid, constant mass flow rate, constant OHTC, constant specific heat, and neglecting the coupling velocity.

The energy conservation between the heat transfer rate through the pipe wall and the fluid thermal energy change as the fluid is cooled by the conduction of heat through the pipe to the sea environment is expressed as follows

$$UdA(T_m - T_o) = -\dot{m}c_p dT_m$$

Where dA is the surface area of the pipeline, $dA = \pi D dx$, $\dot{m}$ is the mass flow rate of the internal fluid, c_p is the specific heat capacity of the internal fluid, T_m is the mean temperature of the fluid, and U is the OHTC, and T_o is the ambient temperature of the pipe's surroundings.

Where

$$U = \frac{1}{A_r\left[\frac{1}{A_i h_i} + \sum_{m=1}^{n} \frac{\ln(r_{m+1}/r_m)}{2\pi L k_m} + \frac{1}{A_o h_o}\right]} \tag{2.16}$$

Where h_i is the film coefficient of the pipeline's inner surface, h_o is the film coefficient of the outer surface, A_i is the pipeline's inner surface area, A_o is the pipeline's outer surface area, A_r is the area of the pipeline at a reference radius, r_m is the radius of layer m, and k_m is the thermal conductivity of layer m.

Separating the variables and integrating from the pipeline inlet to the point with pipe length of x from the inlet

$$\int_{T_{in}}^{T(x)} \frac{dT_m}{T_m - T_o} = \int_0^x -\frac{U\pi D dx}{\dot{m}c_p}$$

After integrating the above equation, the temperature profile equation is as follows

$$T(x) = T_o + (T_{in} - T_o)\exp(-\frac{U\pi Dx}{\dot{m}c_p})$$

Where T_{in} is the inlet temperature of the fluid, and $T(x)$ is the temperature of the fluid at distance x from the inlet.

2.4 Dataset used

This comparison uses the dataset that was presented in Bai et al. and is shown in Table 2.2. Moreover, the comparison focuses on the effect of changing the mass flow rate and changing the length of the pipeline as present in Table 2.3.

Table 2.3: Different cases addressed in the study

	Case 1	Case 2	Case 3	Case 4
Fluid Flow rate $\dot{m}$ m^3/d	3006 m^3/d (Low)	3006 m^3/d (Low)	7950 m^3/d (High)	7950 m^3/d (High)
Pipeline Length L m	8,000 m (Short)	80,000 m (Long)	8,000 m (Short)	80,000 m (Long)

2.5 Comparison between the Approximate and Analytical Solutions

In this subsection, a comparison is conducted of the approximate and analytical solutions using the dataset presented in Table 2.2 in the case of a steel pipeline. The contribution of this subsection is to conduct a comprehensive comparison under different cases to find the best solution to predict the temperature profile in steel pipelines. The cases are obtained by varying the length of the pipeline and the flow rate of the fluid inside (as described in Table 2.3). All the code used to run the experiments was implemented in MATLAB R2017.

Case 1: Low flow rate in case of short pipelines

In this case, the flow rate of the fluid inside the steel pipeline is set to 3006 m^3/d and the length of the pipeline between the inlet and the outlet is 8000 m. Figure 2-4 shows the results of the comparison between the approximate and analytical solutions in this case.

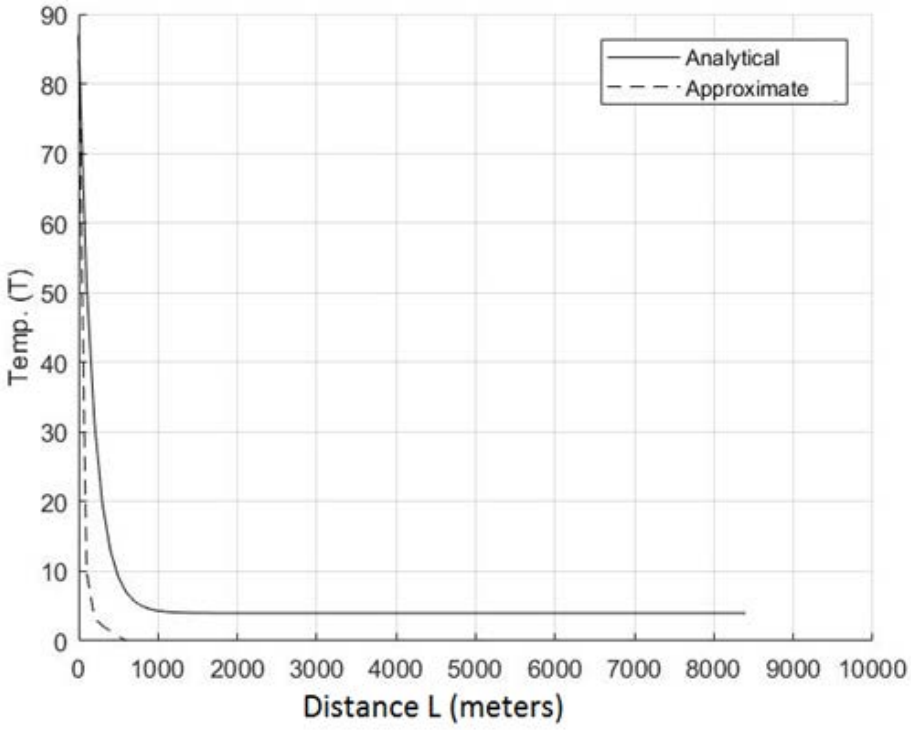

Figure 2-4: Approximate vs. Analytical solution in case 1 (low flow rate, short pipeline)

Case 2: Low flow rate in case of long pipelines

In this case, the flow rate of the fluid inside the steel pipeline is set to 3006 m^3/d and the length of the pipeline between the inlet and the outlet is 80000 m. Figure 2-5 shows the results of the comparison between the approximate and analytical solutions in this case.

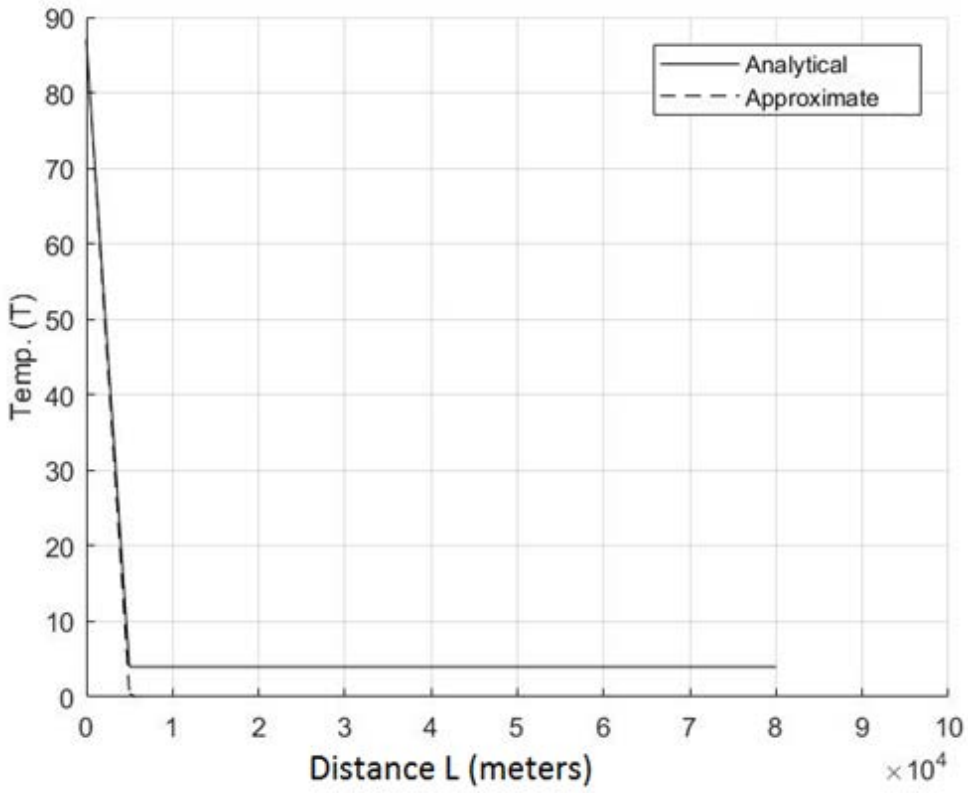

Figure 2-5: Approximate vs. Analytical solution in case 2 (low flow rate, long pipeline)

Case 3: High flow rate in case of short pipelines

In this case, the flow rate of the fluid inside the steel pipeline is set to 7950 m^3/d and the length of the pipeline between the inlet and the outlet is 8000 m. Figure 2-6 shows the results of the comparison between the approximate and analytical solutions in this case.

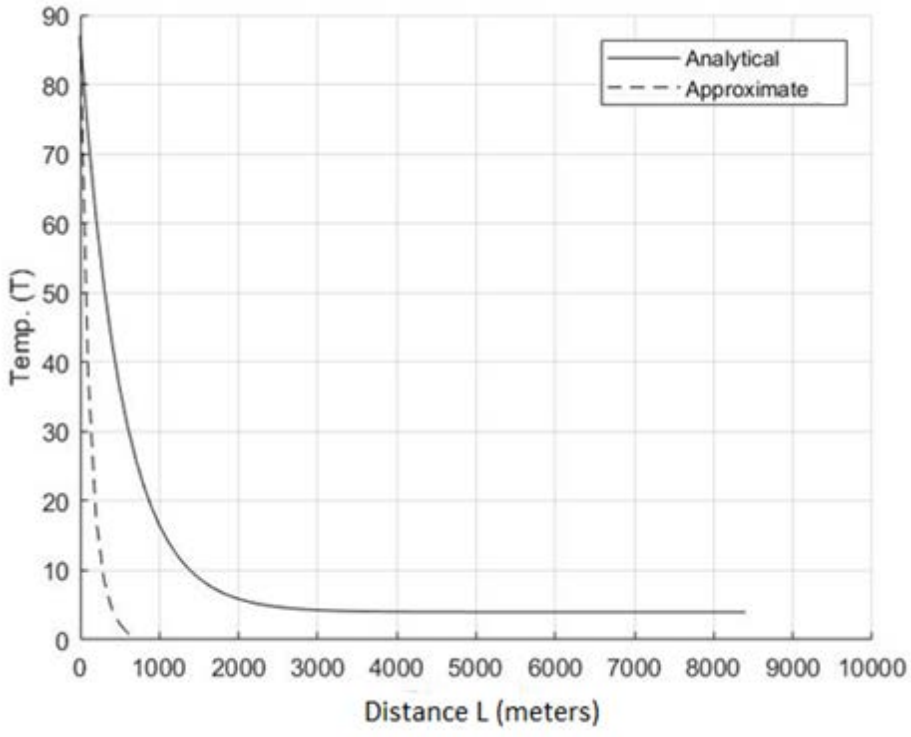

Figure 2-6: Approximate vs. Analytical solution in case 3 (high flow rate, short pipeline)

Case 4: High flow rate in case of long pipelines

In this case, the flow rate of the fluid inside the steel pipeline is set to 7950 m^3/d and the length of the pipeline between the inlet and the outlet is 80000 m. Figure 2-4 shows the results of the comparison between the approximate and analytical solutions in this case.

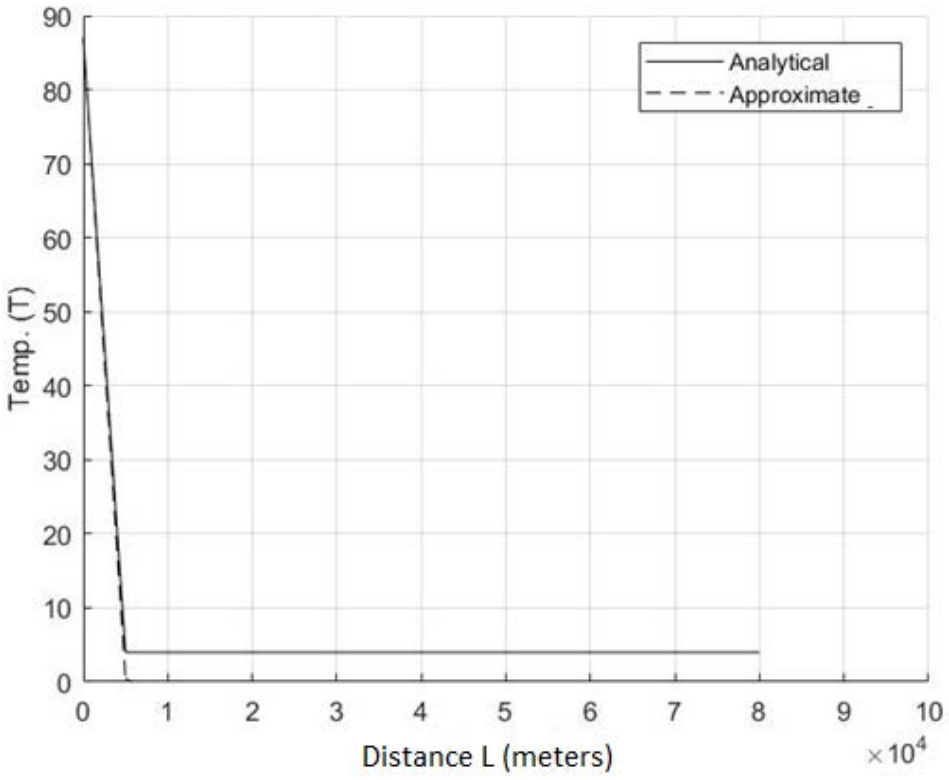

Figure 2-7: Approximate vs. Analytical solution in case 4 (high flow rate, long pipeline)

2.5.1 Results Discussion

In this comparison, the data presented in Table 2.2 is used to find the temperature profile using the two solution models in the case of steel pipelines. The flow rate (low vs. high) and the pipeline length (short vs. long) are varied, which results in 4 different cases as shown in Table 2.3.

Figure 2-4 shows that the approximate solution produces a profile in which the temperature rapidly drops to -2.8467℃ at a length of 1000m. Not only did the temperature decrease past the ambient temperature, but it continued to drop. Whereas, the analytical solution produces a profile in which the temperature drops to 4.0203797℃ at length 1500m and then saturates at that temperature. The analytical solution temperature profile is more accurate because the temperature inside the pipeline saturates at 4^0C which is the ambient temperature. It is logical that the temperature inside the pipeline cannot drop below the ambient temperature unlike what is calculated by the approximate solution.

Figure 2-5 shows that the approximate solution produces a profile in which the temperature rapidly drops to 0.4653280226^0C at a length of 5000m Not only did the temperature decrease past the ambient temperature, but it continued to drop. Whereas, the analytical solution produces a profile in which the temperature drops to 4.000000000076938^0C at length 5000m and then saturates at that temperature. To clarify, why the saturation temperature is different in this case, as opposed to Figure 2-4, despite the fact that it was only a change of length, refer to Equation 2.15 and Equation 2.1. Both equations include the total length of the pipeline (L) either directly, as in Equation 2.15, or indirectly through the inclusion of the thermal gradient (G) which depends on the total length

of the pipeline, as shown in Equation 2.1. By examining Figure 2.5, it is evident that the analytical solution is still more accurate as it saturates to the ambient temperature of 4℃.

In the case of high flow rate (either short pipeline or long pipeline), the analytical solution still provides a better and more accurate temperature profile inside the steel pipeline. This is seen from the fact that the approximate solution predicts a temperature of 0.0083139^0C at $700m$ in the pipeline (Figure 2.6) and -0.193497^0C at 6000 m in the pipeline (Figure 2.7), which is not possible because the temperature of the outside medium is 4℃ and accordingly the fluid flowing in the pipeline should not go below 4℃ degrees.

The objective to perform this comparison is to stress that the analytical solution is more accurate as opposed to Goa [16] who used the approximate solution in oil and gas, his solution is simplified. Hence, it is proved that even the approximate solution will work only in the short pipelines but will not work in case of long pipelines. Based on this discussion, the thesis proposes that the analytical solution is more accurate in predicting the temperature profile inside pipelines and can be applied in cases of short and long pipelines under different flow rates. The approximate solution is inaccurate in long pipelines and it excludes the pipeline materials properties while focusing on the insulation materials properties.

It is worth mentioning that in this comparison a steel pipeline is used which has a high thermal conductivity as shown in Table 2.3, whereas when Guo et al. applied the approximate solution he used different insulations with very low thermal conductivity as shown in Table 2.1. But in the comparison, the thesis proved that the material of the pipeline (in this case steel) has big impact on the temperature profile. This point is continued on in subsection 2.6 by comparing composite pipelines to traditional steel ones.

2.6 Thermal Characteristics Comparison between Composite and Steel

This section focuses on the material of the pipeline and compares the traditional steel to composite pipelines. From the comparison presented in section 2.5 and the results discussion in section 2.5.1, it is evident that the analytical solution is more general in predicting the temperature profile along short and long pipelines with low and high flow rates. Hence, we use the analytical solution in this comparison, where the varying parameter is the material of the pipeline (steel vs. composite).

The comparison also focuses on the effect of changing the mass flow rate and changing the length of the pipeline as present in Table 2.3.

The objective of this thermal characteristics investigation is to predict the fluid flow temperature along the pipeline and calculate the heat loss along the pipeline.

The assumptions used in this comparison are as follows:

- Nominal homogenized mechanical and heat transfer properties are used for composite and steel pipelines.
- The same geometry (thickness and diameter) for both pipelines.

All the code used to run the experiments was implemented in MATLAB R2017 and was run on a Lenovo laptop with a processor i7 and 8 GB Ram.

2.6.1 Dataset used in Steel vs Composite

This comparison uses the data presented in Tables 2.4-2.6. It is worth mentioning that the thermal characteristics of the materials of steel and composite are presented in Table 2.5.

Table 2.4: Dataset used in the steel vs composite comparison [6]

Pipeline outer Diameter D_O	0.219 m
Pipeline wall thickness t	0.0143 m
Fluid Density ρ	795.8 kg/m^3
Fluid specific heat C_p	3054 Jkg^{-1}°C
Entry Fluid Temperature T_s	87°C
Ambient Temperature T_O	4°C

Table 2.5: Thermal characteristics of steel and composite pipelines. Data in this table was taken from [7]

Material	Thermal Conductivity W/mK	Specific Heat J/kgK
Steel Pipe	50	450
Composite Pipe	0.4	1670

Table 2.6: Different cases for comparing steel vs. composite

	Case 1	Case 2	Case 3	Case 4
Fluid Flow rate Q	3006 m^3/d (Low)	3006 m^3/d (Low)	7950 m^3/d (High)	7950 m^3/d (High)
Pipeline Length L	8,000 m (Short)	80,000 m (Long)	8,000 m (Short)	80,000 m (Long)

Case 1: Steel verses composite (low flow rate, short pipelines):

The flow rate inside the pipeline is set to 3006 m^3/d and the length of the pipeline between the inlet and the outlet is 8000m. Figure 2-8 shows the results of the comparison between the steel and composite in this case.

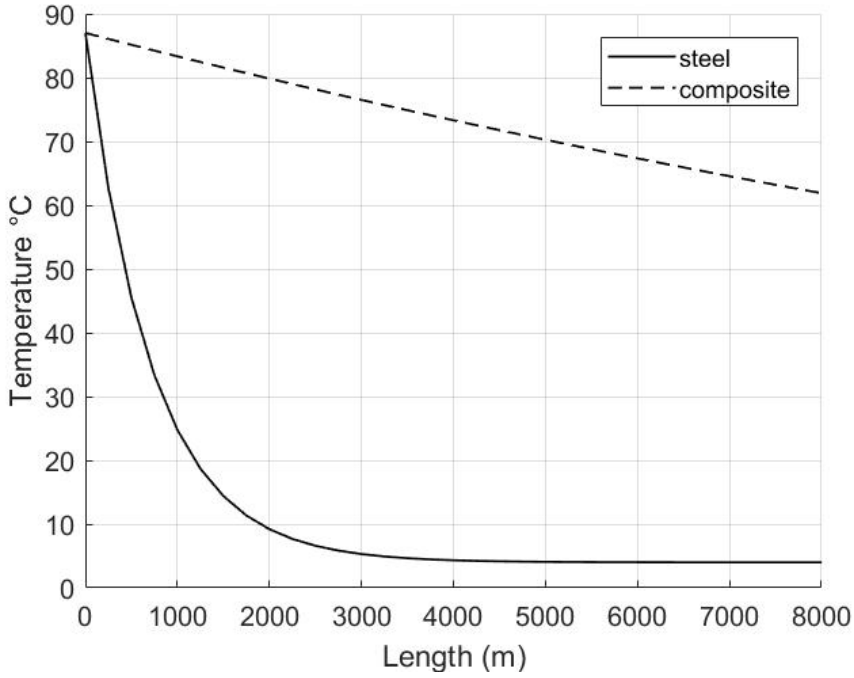

Figure 2-8: Steel vs. composite in case 1 (low flow rate, short pipeline)

Case 2: Steel verses composite (low flow rate, long pipelines):

The flow rate inside the pipeline is set to 3006 m^3/d and the length of the pipeline between the inlet and the outlet is 80000m. Figure 2-9 shows the results of the comparison between the steel and composite in this case.

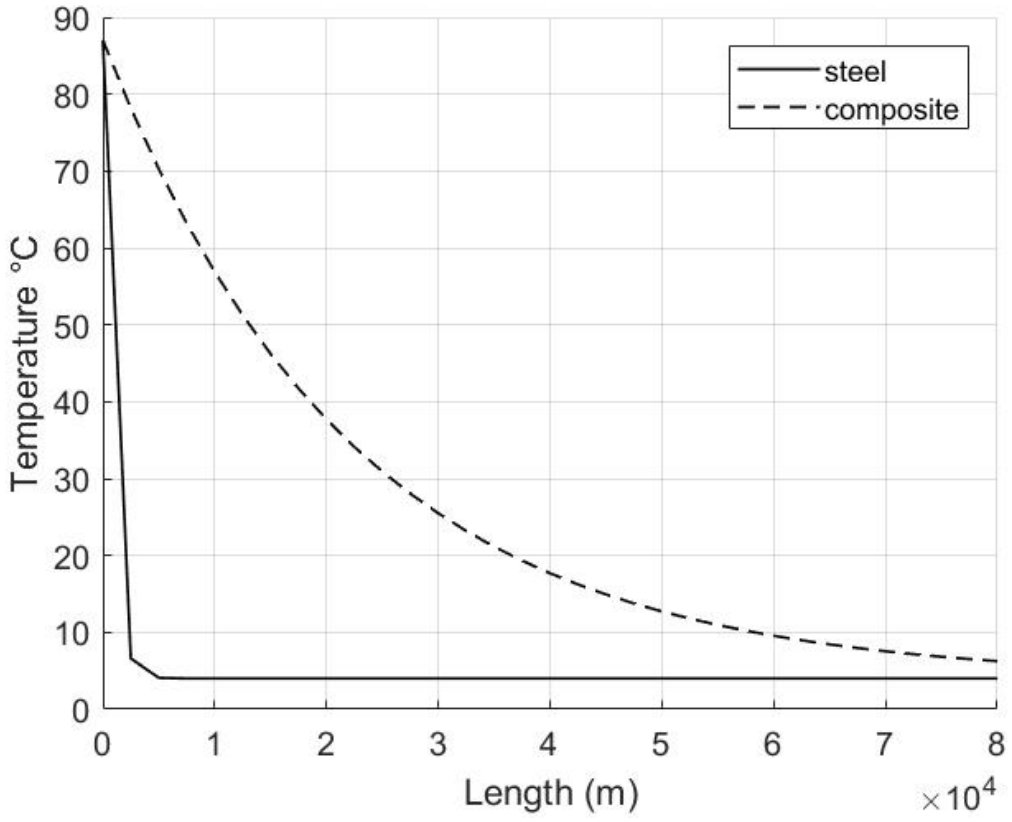

Figure 2-9: Steel vs. composite in case 2 (low flow rate, long pipeline)

Case 3: Steel verses composite (high flow rate, short pipelines):

The flow rate inside the pipeline is set to 7950 m^3/d and the length of the pipeline between the inlet and the outlet is 8000m. Figure 2-10 shows the results of the comparison between the steel and composite in this case.

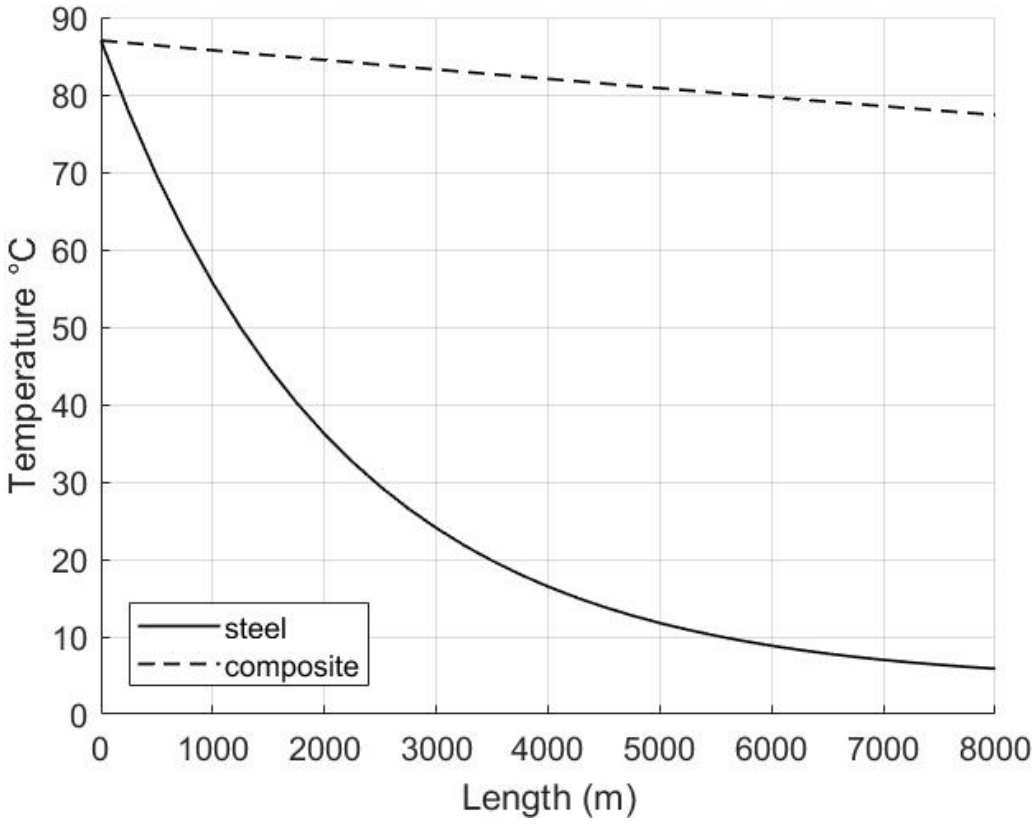

Figure 2-10 Steel vs. composite in case 3 (high flow rate, short pipeline)

Case 4: Steel verses composite (high flow rate, long pipelines):

The flow rate inside the pipeline is set to 7950 m^3/d and the length of the pipeline between the inlet and the outlet is 80000m. Figure 2-11 shows the results of the comparison between the steel and composite in this case.

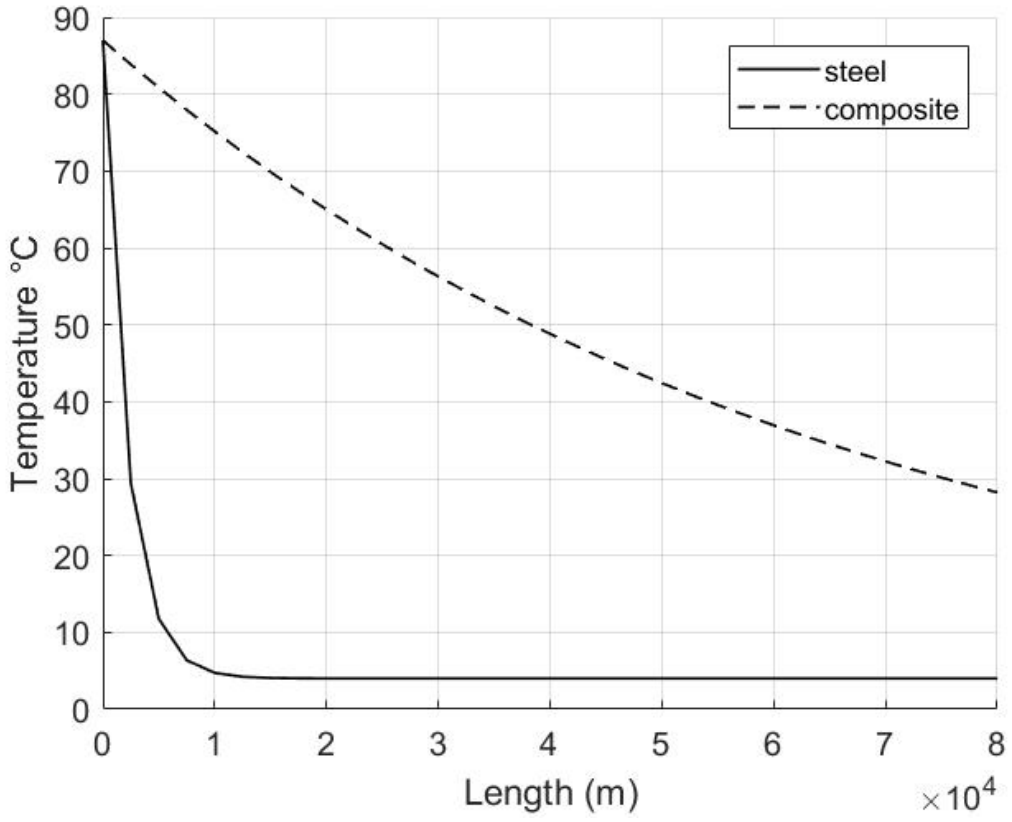

Figure 2-11: Steel vs. composite in case 4 (high flow rate, long pipeline)

2.6.2 Results Discussion

This comparison used the data presented in Table 2.4 and the thermal properties presented in Table 2.5. To show which material has better thermal characteristics, the flow

rate (low vs high) and the pipeline length (short vs long) are varied, which results in 4 different cases as shown in Table 2.6.

Figure 2-8 shows that the composite pipeline temperature rapidly drops to 57.49℃ at a length of 8000m. Whereas, the steel pipeline temperature rapidly drops to 4.0001℃ at length 8000m. Figure 2-9 shows that the composite pipeline temperature rapidly drops to 5.025℃ at a length of 80000m. Whereas, the steel pipeline temperature rapidly drops to 4.0℃ at length 80000m. Figure 2-10 shows that the composite pipeline temperature rapidly drops to 75.422℃ at a length of 8000m. Whereas, the steel pipeline temperature rapidly drops to 4.8℃ at length 8000m. Finally, Figure 2-11 shows that the composite pipeline temperature rapidly drops to 22.47℃ at a length of 80000m. Whereas, the steel pipeline temperature rapidly drops to 4℃ at length 80000m.

Based on this discussion, the thesis proposes that the composite pipeline has superior thermal characteristics compared to the steel pipeline.

2.7 Heat loss Calculation

This section presents the results for the heat loss calculations based on case 1: low flow rate and short pipeline.

The mathematical equation of heat loss Q is defined according to [6] as

$$Q = UA\Delta T \tag{2.16}$$

In the case of a steel pipeline, the heat loss is defined as

$$Q_s = U_s A_s \Delta T_s \tag{2.17}$$

And the heat loss equation along the composite pipeline is defined as

$$Q_c = U_c A_c \Delta T_c \tag{2.18}$$

To find the heat loss ratio between steel and composite, divide Equation 2.17 by Equation 2.18. Since the steel and composite pipelines have the same geometry, then A_s and A_c are equal and thus, the heat loss ratio between the steel pipeline and composite becomes

$$\frac{Q_s}{Q_c} = \frac{U_s \Delta T_s}{U_c \Delta T_c} \tag{2.19}$$

Substituting in Equation 2.19 with the values taken from Figure 2-11, results in the following heat loss ratio

$$\frac{Q_s}{Q_c} = 44.8$$

Table 2.7: Heat loss calculations based on the full length of the pipeline (low flow rate, short pipeline)

	Steel	Composite
Heat loss along the pipeline W	$3.579*10^9$	$0.116059*10^9$
Heat loss along the pipeline W/weight	$454.76*10^3$	$62.73*10^3$

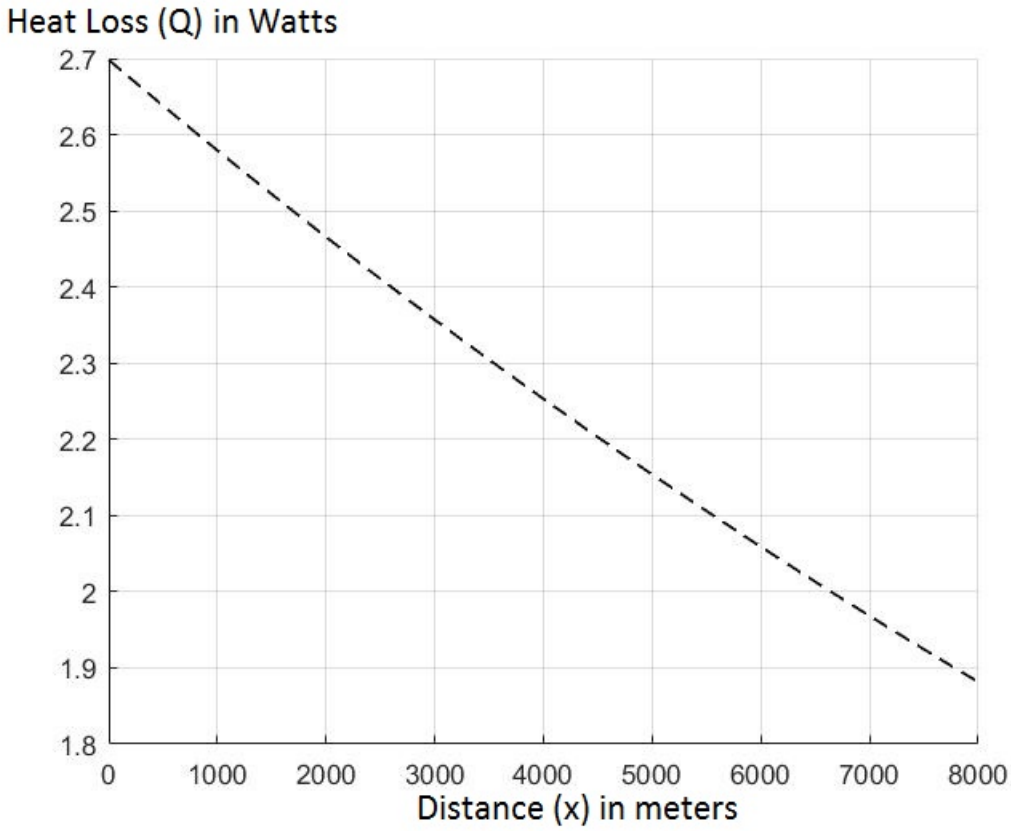

Figure 2-12: Heat loss calculations profile along a composite pipeline (low flow rate, short pipeline)

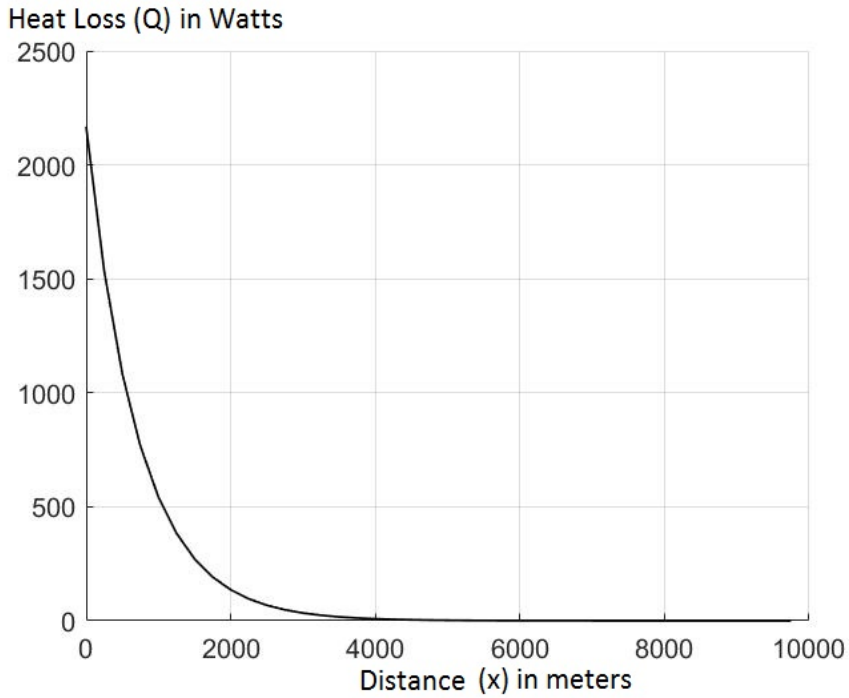

Figure 2-13: Heat loss calculations profile along a steel pipeline (low flow rate, short pipeline)

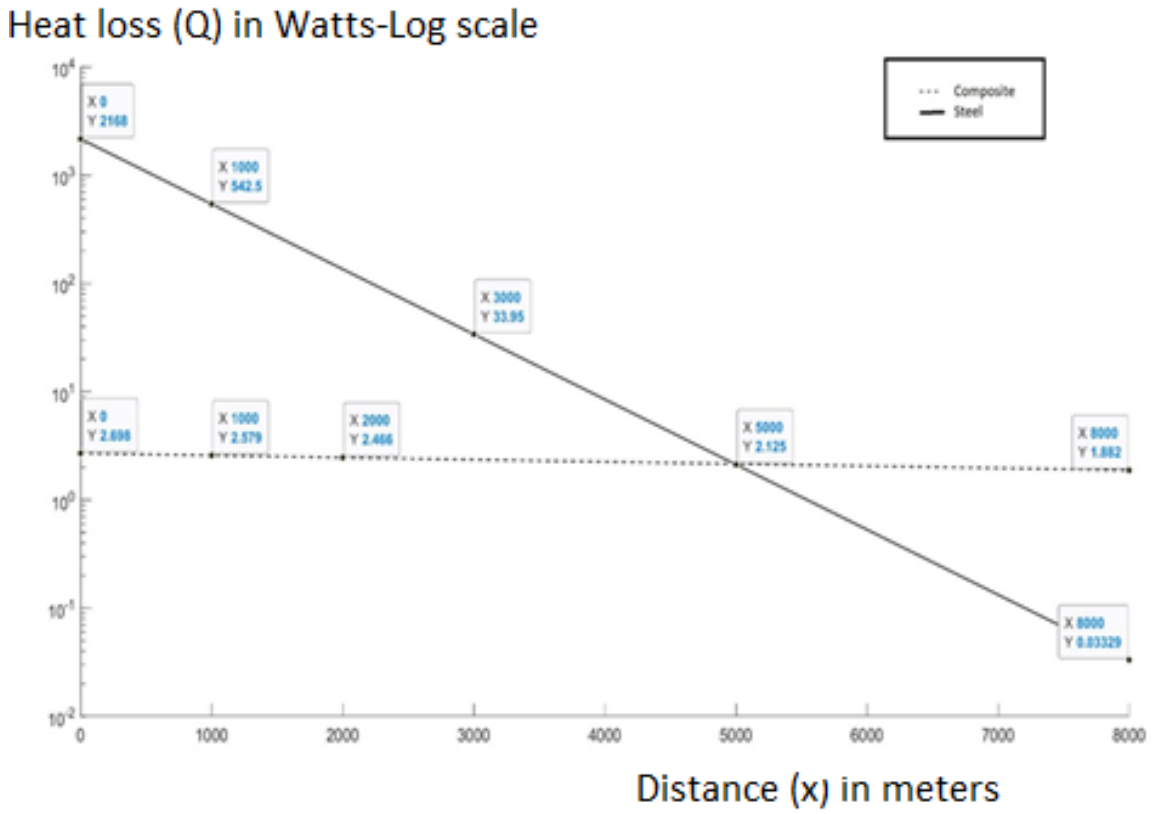

Figure 2-14: Log scale heat loss (low flow rate, short pipeline)

Figures 2-12 and 2-13 show the heat loss (Q) decay in case of CCR and SCR. Figure 2-12 describes a linear decay of Q in case of composite catenary riser whereas Figure 2-13 describes exponential decay of heat loss in case of SCR.

In the log scale heat loss Figure 2-14, it is seen that in the case of composite, the difference in temperature from one point to the next is almost constant ($500m$), hence the heat loss is almost constant. On the other hand, in the case of steel, the temperature difference varies from one point to the next, and hence the heat loss exhibits an exponential decay.

Based on the results, the composite pipeline has superior thermal characteristics compared to steel pipeline.

Chapter 3 : Mechanical Considerations

3.1 Introduction

As observed in the previous chapter, thermal characteristics of composite materials can be easily described with heat transfer models. In other words, they do pose further difficulty beyond the analysis of steel pipelines. Additionally, design and failure analysis of composite materials is distinctly different from their metal counterparts. The objective of this chapter is to conduct a comparison between steel and composite pipes based on mechanical considerations.

For many years, steel catenary risers (SCR) were considered as the best solution for deep-water operations due to their lower cost and significant dynamic resistance. However, they suffered from many disadvantages including heavy weight, low corrosion resistance, and high thermal conductivity. Recently, many designers proposed to use composite catenary risers (CCR) instead of SCR. Composite materials are consider superior over their metallic counterparts because of their better thermal characteristics, high strength, low density, light weight, high corrosion resistance, excellent fatigue properties, and lower coefficient of thermal expansion (CTE) [19]. These advantageous properties favor using composite materials in catenary risers.

Salama et al. [20-23], ground breaking researchers in this field, proposed composites as preferred materials for pipelines. They also proposed particular designs for composites to overcome environment.

In [20], the authors studied the benefits of switching heavy steel tendon to the lightweight composite tendon and the economic benefits of using composite risers instead of the steel risers. One of the most important benefits of high thermal insulation is to guarantee flow assurance. In the discussion, the authors argued that although a composite part costs twice that of its equivalent steel part, the composite weight is half the equivalent steel part, and in the long run both will have the same overall cost. Also, Salama et al. focus on evaluating the potential of composite materials for TTR (Top Tensioned Riser) systems from the standpoint of possible impact on overall cost and reliability [21]. In [23], the paper described the first installation of a full size high-pressure composite drilling riser joint, and using it to drill three wells while located at different positions along the riser string. Another study by Salama et al. [22] conducted different assessment tests. The work concluded that it is possible to manufacture composite riser joints that meet all mandatory design requirements and can be installed successfully, even in ultra-deep-water environments.

3.2 Mechanics of Composites

In steel pipelines, the mechanics focus on the study of the stress, strain, deformation, and failure due to the mechanical and thermal loads. On the other hand, the composites' mechanics are more complicated compared to steel. This is because each composite consists of two or more different materials with different properties, mainly, fiber and resin. These are combined in the micro- or macro-scale, to form a new material with different properties. Originally fibers and resin are assumed to be homogenous and isotropic. Once they are combined in one layer it becomes neither homogeneous nor isotropic. Best case scenario, one layer is assumed to be orthotropic. Moreover, as different layers are stacked (with each layer

having its own orthotropic properties and orientation adding the possibly different material in hybrid composites), the formed laminate would have new “collective” characteristics and properties. This briefly demonstrates the challenge of composites based on mechanics, hence the need for thorough studies as would be described in the next subsections. In general, the mechanics of composite materials are divided into:

1. The micromechanics study: Studies the effect on or the change of properties of the composite material as a result of its components interaction. The interaction between the components in micromechanics is usually studied on a microscopic scale. The micromechanics study may enable predicting failure mode in composite materials. Most importantly, failure is initiated in the microscale then propagates to the macroscale.
2. The macromechanics study: Studies the behavior of composite materials (as laminate) due to mechanical and thermal loads. Mathematical models are developed to express composite material response to loads on the macroscopic scale.

In brief, the study of the mechanics of composite materials can help designers optimize utilizing the properties of composite materials to meet the design requirements. This process is normally called “tailoring” composites to meet design requirements and constraints. This is one of the many advantages for composites beyond their superior specific strength.

3.2.1 Manufacturing

As stated earlier composite materials consist of two or more different materials with different properties combined to form laminate with collective different and new properties. The manufacturing of a composite structure includes using a large number of fibers arranged into a thin layer of matrix to form a lamina (also called a ply) [19]. A composite material consists of:

1. Fiber: It is considered the main load carrier and reinforces the matrix. There are various types of fibers such as carbon fiber, glass fiber, aramid fiber E-glass fiber, S-glass fiber, and etc. Designers change the fiber orientation in each layer as well as the stacking sequence to generate a wide range of physical and mechanical properties. Fibers have different forms, as shown in Figure 3-1, such as unidirectional continuous, multidirectional continuous, random discontinuous, and etc. This can be summarized in two main categories, namely, continuous being unidirectional or woven and discontinuous being chopped aligned or in random orientation.
2. Matrix: It supports and protects the fiber. Different types of matrixes include polymer (e.g. epoxy and polyester), metallic (e.g. aluminum and copper), carbon, ceramic, etc. In fiber-reinforced composite, the matrix serves various purposes including maintaining the fibers in place, transferring the stress between the fibers, providing a barrier against adverse environment (e.g. chemicals and moisture), protecting the surface of the fibers from mechanical degradation, and finally, providing lateral support against the possibility of fiber buckling under compressive loads.

Laminae

As defined in [19], a Lamina is a thin ply or layer (with thickness of 0.1to 1 mm) which consists of fibers arranged in a matrix. A lamina is a flat (can drape into a curved shape, like a thin shell) arrangement of unidirectional or woven fibers in a supporting matrix. Depending on manufacturing specifications and matric and fiber materials a lamina may have a different thickness, different fiber material and sometimes different matrix material. Meanwhile a laminae is the plural of lamina and it refers to an arrangement of set or several lamina. Laminae can also be used to refer to a laminate before matrix consolidation or polymerization process. This process is commonly referred as curing

Laminate

A laminate is a bonded stack of laminae with various orientations relative to principal material directions in the laminae. Each laminae is bonded to the other by the same matrix material that is used to support the fibers in each ply. The laminate is made by stacking a number of thin layers of fibers and matrix and consolidating them into desired thickness [24].

Stacking

The exact stacking sequence affects the collective mechanical properties of a laminate. In other words, based on stacking sequence the extension, bending and torsional as well as their coupled stiffness parameters would change and hence, the collective strength and stiffness of the laminate. An example on elastic coupling (coupling in stiffness) is when applying tension on a flat laminate the laminate would undergo torsional deformation. This is referred to as “extension-twist coupling”. Elastic coupling is also advantageous for

tailoring the properties to best fit design requirements and constraints in advanced applications, e.g. rotor wing. Meanwhile in majority of engineering applications it is desired to eliminate elastic coupling from the design when it is not required. Therefore symmetric stacking sequence is followed to allow the coupling stiffness matrix to be trivial, i.e. $B = 0$. This process will be explained in detail in the following section. It should be noticed that symmetric stacking should alleviate coupling under both mechanical and thermal loads. Meanwhile coupling under thermal loads is more complicated than under mechanical ones. The stacking of layers starts from the top of the laminate. Also, the stacking sequence gives the orientation of fibers with respect to global axis in degrees. The next section proposes symmetric laminae with the following stacking sequence $[90 \quad /\pm 45 \ / \quad 0]_s$.

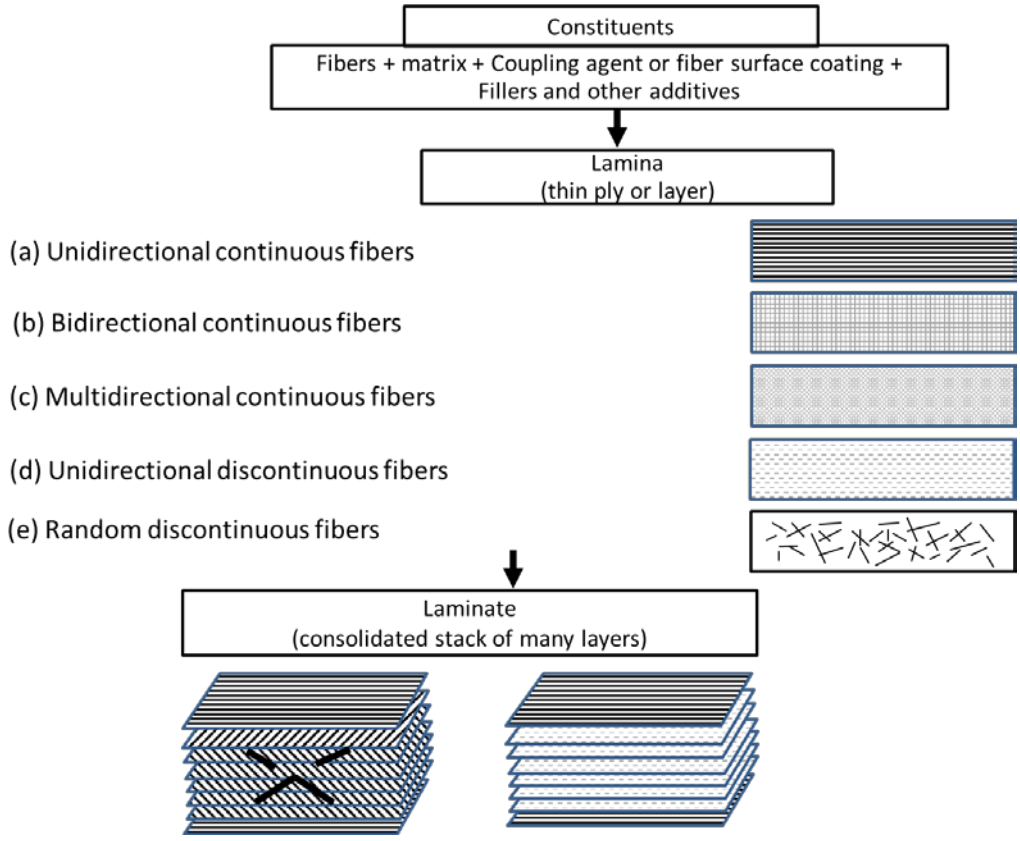

Figure 3-1: Structure of fiber-reinforced composite [19]

Filament Winding

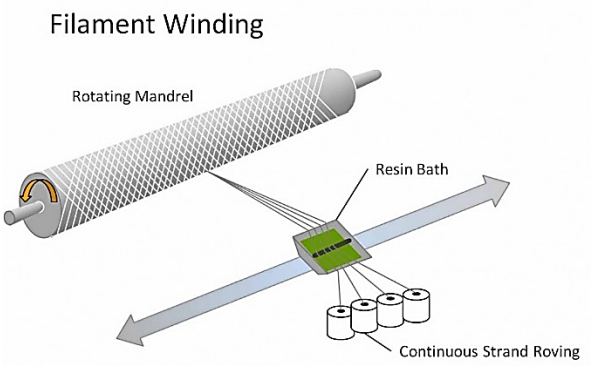

Figure 3-2: Filament Winding process, picture courtesy of [25]

Filament winding is traditional and special technique used for a structures with near-symmetry in terms of geometry (such as a pipeline, pressure vessel, fuel tanks, etc.). As shown in Figure 3-2, the fibers are pulled off by the rotation of a mandrel passing through a resin bath then the fiber are wound or placed around the rotation structure. The mold of the structure is rotating at certain speed while the carriage pulling and placing the fibers is moving at different speed (along the axis of the mandrel). Adjusting both speeds (rotational of the mandrel and translational of the carriage) enable stacking the fibers over the mandrel in the desired stacking sequence [26]. The manufacturing of a long pipeline using fiber winding is shown in Figure 3-3. This is consistent with Salama et al [22] when they discuss in their paper that "*the carbon fibers and E-glass fibers rovings are impregnated with uncured epoxy resin bath*" by using the winding technique. Picard et al [27] also present in their paper that "*The pipeline fabrication process involves winding specially pre-impregnated carbon reinforced carbon layers around the liner with a specific angle*".

Figure 3-3: Long pipeline manufacturing, figure courtesy of [27]

3.2.2 Classical Lamination Theory

As stated earlier, mathematical modeling in the macroscale is needed to enable calculating different stiffness parameters of a laminate or composite structure. This mathematical model is referred to as the Classical Lamination Theory (CLT). This theory accounts for the stacking of several laminae with different material properties and different orientations. It also takes advantage of plane stress assumption to simplify the mathematical model and reduce the size of the linear algebra problem. In the meantime CLT is a simplified version of the Kirchhoff-Love [28, 29] thin plate theory. Therefore, CLT inherits the assumptions of the Kirchhoff-Love plate theory (contrasting deformed to undeformed configurations). All assumptions are geometric and applied to a straight line normal to the mid-plane of the laminate (or plate).

1. Straight line normal to midplane remains normal to midplane
2. Straight line normal to midplane remains straight
3. Straight line normal to midplane is rigid (with no change in its length).

In addition to the Kirchhoff-Love assumptions mentioned above, the following assumptions are added for the classical lamination theory (CLT) [30]:

1. Perfect bonding between different laminae.
2. Linear and continuous strain distribution across the laminate thickness.
3. Each laminae can be isotropic, orthotropic or transversely isotropic.
4. The laminate thickness is too small comping to its width ($t << L$).
5. Each laminae is considered to be uniform thickness.
6. Each laminae is in the state of plane stress (assumption valid for thin structures).

Mathematical Model of CLT

The mathematical model provided by the CLT is provided in this subsection as introduced in [19], [24], and [30]. Figure 3-4 provides a sketch of a laminated plate under general loading conditions. The objective is to study stresses and strains developed in this plate due to applied loading. Therefore, it is essential to assume a displacement field to describe the manner in which this laminate (or plate) would deform. Assuming small deformation and linear elastic behavior a linear displacement field can be adopted.

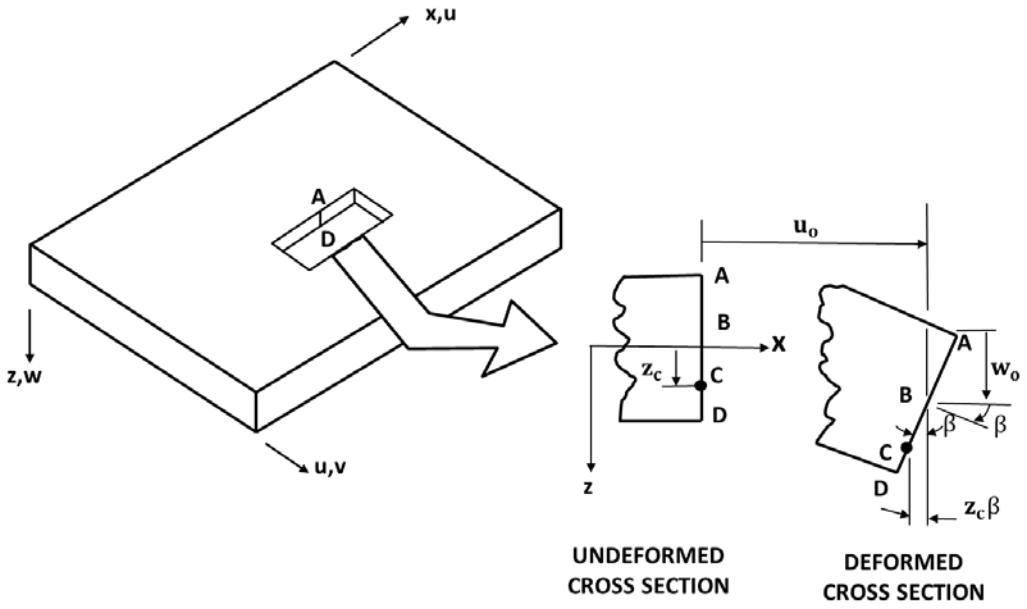

Figure 3-4 Geometry of deformation in x-z plane [24]

The displacement u at any point z through laminate thickness is

$$u = u_o - z\frac{\partial w_o}{\partial x} \tag{3.1}$$

The displacement v at any point in the y direction is

$$v = v_o - z\frac{\partial w_o}{\partial y} \tag{3.2}$$

Where the transvers displacement $w = w_o(x, y)$. Meanwhile, the laminate strains are defined as

$$\varepsilon_x = \frac{\partial u}{\partial x}$$

$$\varepsilon_y = \frac{\partial v}{\partial y} \tag{3.3}$$

$$\gamma_{xy} = \frac{\partial u}{\partial y} + \frac{\partial v}{\partial x}$$

Substituting Equations 3.3 into Equations 3.1 and 3.2 yields

$$\varepsilon_x = \frac{\partial u_o}{\partial x} - z\frac{\partial^2 w_o}{\partial x^2}$$

$$\varepsilon_y = \frac{\partial v_o}{\partial y} - z\frac{\partial^2 w_o}{\partial y^2} \tag{3.4}$$

$$\gamma_{xy} = \frac{\partial u_o}{\partial y} + \frac{\partial v_o}{\partial x} - 2z\frac{\partial^2 w_o}{\partial xy}$$

Therefore the strain field can be expressed in terms of midplane strains and curvatures as follow

$$\begin{bmatrix} \varepsilon_x \\ \varepsilon_y \\ \gamma_{xy} \end{bmatrix} = \begin{bmatrix} \varepsilon^o{}_x \\ \varepsilon^o{}_y \\ \gamma^o{}_{xy} \end{bmatrix} + \begin{bmatrix} \kappa_x \\ \kappa_y \\ \kappa_{xy} \end{bmatrix} \tag{3.5}$$

Where ${\varepsilon^o}_x$ and ${\varepsilon^o}_y$ are midplane normal strains and ${\gamma^o}_{xy}$ is the shear strain are

$$\begin{bmatrix} {\varepsilon^o}_x \\ {\varepsilon^o}_y \\ {\gamma^o}_{xy} \end{bmatrix} = \begin{bmatrix} \frac{\partial u_o}{\partial x} \\ \frac{\partial v_o}{\partial y} \\ \frac{\partial u_o}{\partial y} + \frac{\partial v_o}{\partial x} \end{bmatrix} \tag{3.6}$$

The κ_x and κ_y are midplane bending and κ_{xy} twisting curvatures are expressed as

$$\begin{bmatrix} \kappa_x \\ \kappa_y \\ \kappa_{xy} \end{bmatrix} = -\begin{bmatrix} \frac{\partial^2 w_o}{\partial x^2} \\ \frac{\partial^2 w_o}{\partial y^2} \\ 2\frac{\partial^2 w_o}{\partial xy} \end{bmatrix} \tag{3.7}$$

Since the stress-strain relations for multilayered laminate can be defined as follows

$$\{\sigma\}_k = [\bar{Q}]_k \{\varepsilon\}_k$$

Where k is the number of layers in a multilayered laminate and $[\bar{Q}]$ is the reduced stiffness matrix at arbitrary orientation θ. Plane stress assumption enabled obtaining the reduced stiffness matrix $[Q]$ for a transversely isotropy material. Using stress and strain transformation rules between the global load application coordinates and local lamina coordinates enabled obtaining $[\bar{Q}]$ from $[Q]$. Substituting this stress-strain relationship into Equation 3.5 allows the stresses in the k^{th} layer to be expressed in terms of laminate middle-surface strain curvature as:

$$\begin{Bmatrix}\sigma_x\\ \sigma_y\\ \tau_{xy}\end{Bmatrix}=\begin{pmatrix}\bar{Q}_{11} & \bar{Q}_{12} & \bar{Q}_{16}\\ \bar{Q}_{12} & \bar{Q}_{22} & \bar{Q}_{26}\\ \bar{Q}_{16} & \bar{Q}_{26} & \bar{Q}_{66}\end{pmatrix}\left(\begin{Bmatrix}{\varepsilon^o}_x\\ {\varepsilon^o}_y\\ {\gamma^o}_{xy}\end{Bmatrix}+z\begin{Bmatrix}\kappa_x\\ \kappa_y\\ \kappa_{xy}\end{Bmatrix}\right) \tag{3.8}$$

Resultant laminate forces and moments can be obtained by integrating through the thickness

$$N_x=\int_{-t/2}^{t/2}\sigma_x dz$$

$$M_x=\int_{-t/2}^{t/2}\sigma_x z dz$$

Where N_x and M_x are the forces and moments per unit width, respectively. These applied force and moment resultants are shown in Figure 3-5 over an element of spatial dimension $(\Delta x, \Delta y)$.

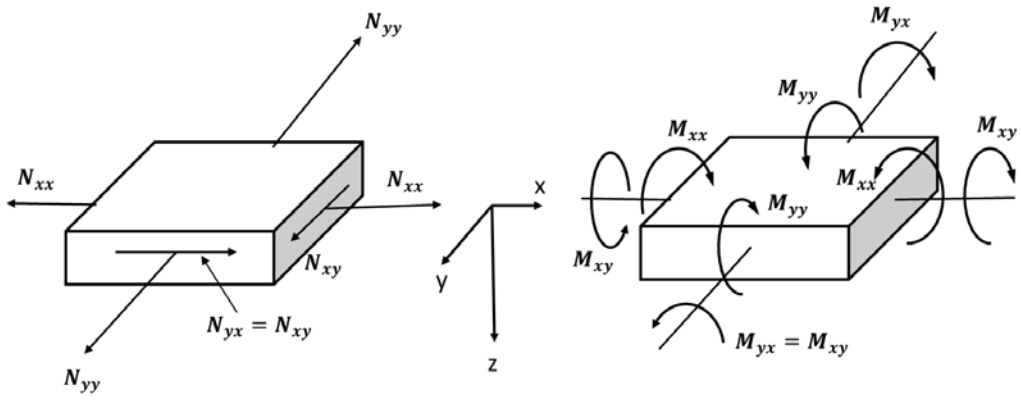

Figure 3-5: Applied force and moment resultant, [19]

Substituting of stresses into these equations the applied force and moment resultants can be expressed as

$$\begin{Bmatrix} N_x \\ N_y \\ N_{xy} \end{Bmatrix} = \int_{-t/2}^{t/2} \begin{Bmatrix} \sigma_x \\ \sigma_y \\ \tau_{xy} \end{Bmatrix} dz = \sum_{j=1}^{N} \int_{h_{j-1}}^{h_j} \begin{Bmatrix} \sigma_x \\ \sigma_y \\ \tau_{xy} \end{Bmatrix}_j dz \tag{3.9}$$

$$\begin{Bmatrix} M_x \\ M_y \\ M_{xy} \end{Bmatrix} = \int_{-t/2}^{t/2} \begin{Bmatrix} \sigma_x \\ \sigma_y \\ \tau_{xy} \end{Bmatrix} z dz = \sum_{j=1}^{N} \int_{h_{j-1}}^{h_j} \begin{Bmatrix} \sigma_x \\ \sigma_y \\ \tau_{xy} \end{Bmatrix}_j z dz \tag{3.10}$$

It is easily noticed that stress is pricewise continuous within each lamina. The integration through the thickness can be expressed as the total sum of piecewise integration through the thickness of each lamina. A sketch for the ***N***-layered laminate is shown in Figure 3-6.

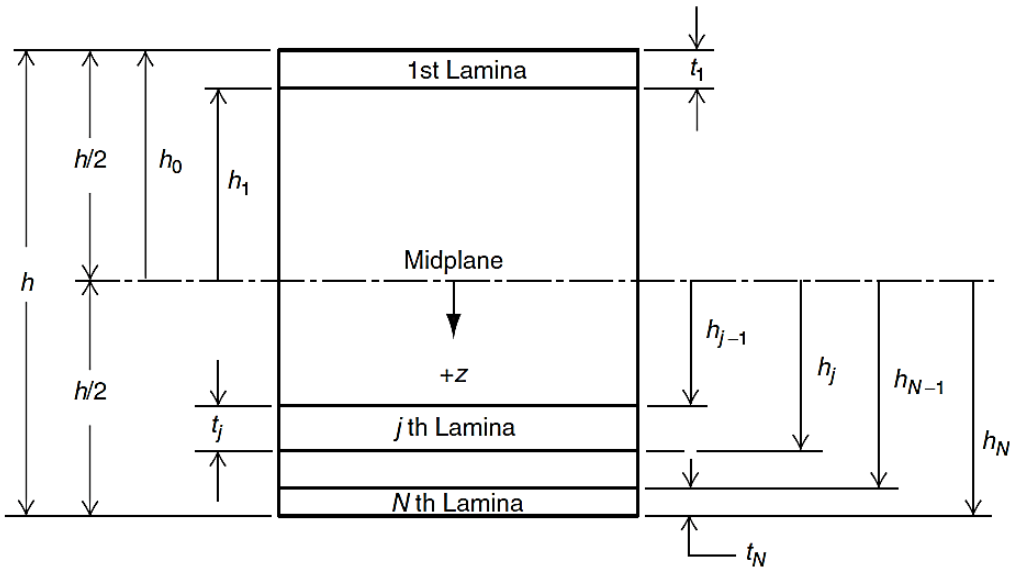

Figure 3-6:Geometry of an *N*-Layered Laminate [19]

By substituting Equation 3.8 into Equation 3.9 and Equation 3.10, the resultant forces and momentum matrix notation become Equations 3.11 and 3.12.

$$\begin{Bmatrix} N_x \\ N_y \\ N_{xy} \end{Bmatrix} = \sum_{j=1}^{N} \left\{ \int_{h_{j-1}}^{h_j} \begin{bmatrix} \bar{Q}_{11} & \bar{Q}_{12} & \bar{Q}_{16} \\ \bar{Q}_{12} & \bar{Q}_{22} & \bar{Q}_{26} \\ \bar{Q}_{16} & \bar{Q}_{26} & \bar{Q}_{66} \end{bmatrix}_j \left(\begin{Bmatrix} {\varepsilon^o}_x \\ {\varepsilon^o}_y \\ {\gamma^o}_{xy} \end{Bmatrix} + z \begin{Bmatrix} \kappa_x \\ \kappa_y \\ \kappa_{xy} \end{Bmatrix} \right) dz \right\} \tag{3.11}$$

$$\begin{Bmatrix} M_x \\ M_y \\ M_{xy} \end{Bmatrix} = \sum_{j=1}^{N} \left\{ \int_{h_{j-1}}^{h_j} \begin{bmatrix} \bar{Q}_{11} & \bar{Q}_{12} & \bar{Q}_{16} \\ \bar{Q}_{12} & \bar{Q}_{22} & \bar{Q}_{26} \\ \bar{Q}_{16} & \bar{Q}_{26} & \bar{Q}_{66} \end{bmatrix}_j \left(\begin{Bmatrix} {\varepsilon^o}_x \\ {\varepsilon^o}_y \\ {\gamma^o}_{xy} \end{Bmatrix} + z \begin{Bmatrix} \kappa_x \\ \kappa_y \\ \kappa_{xy} \end{Bmatrix} \right) z\, dz \right\} \tag{3.12}$$

Since the stiffness matrix for the lamina is often constant and the midplane strains and curvatures are constants, hence they can be taken outside the integration. Equations 3.11 and 3.12 can be rearranged as:

$$\begin{Bmatrix} N_x \\ N_y \\ N_{xy} \end{Bmatrix} = \sum_{j=1}^{N} \left\{ \begin{bmatrix} \bar{Q}_{11} & \bar{Q}_{12} & \bar{Q}_{16} \\ \bar{Q}_{12} & \bar{Q}_{22} & \bar{Q}_{26} \\ \bar{Q}_{16} & \bar{Q}_{26} & \bar{Q}_{66} \end{bmatrix}_j \left(\begin{Bmatrix} {\varepsilon^o}_x \\ {\varepsilon^o}_y \\ {\gamma^o}_{xy} \end{Bmatrix} \int_{h_{j-1}}^{h_j} dz + \begin{Bmatrix} \kappa_x \\ \kappa_y \\ \kappa_{xy} \end{Bmatrix} \int_{h_{j-1}}^{h_j} z dz \right) \right\} \tag{3.13}$$

$$\begin{Bmatrix} M_x \\ M_y \\ M_{xy} \end{Bmatrix} = \sum_{j=1}^{N} \left\{ \begin{bmatrix} \bar{Q}_{11} & \bar{Q}_{12} & \bar{Q}_{16} \\ \bar{Q}_{12} & \bar{Q}_{22} & \bar{Q}_{26} \\ \bar{Q}_{16} & \bar{Q}_{26} & \bar{Q}_{66} \end{bmatrix}_j \left(\begin{Bmatrix} {\varepsilon^o}_x \\ {\varepsilon^o}_y \\ {\gamma^o}_{xy} \end{Bmatrix} \int_{h_{j-1}}^{h_j} z dz + \begin{Bmatrix} \kappa_x \\ \kappa_y \\ \kappa_{xy} \end{Bmatrix} \int_{h_{j-1}}^{h_j} z^2 dz \right) \right\} \tag{3.14}$$

Equations 3.13 and 3.14 can also be presented as Equations 3.15 and 3.16

respectively.

$$\begin{Bmatrix} N_x \\ N_y \\ N_{xy} \end{Bmatrix} = \sum_{j=1}^{N} \left\{ \begin{bmatrix} \bar{Q}_{11} & \bar{Q}_{12} & \bar{Q}_{16} \\ \bar{Q}_{12} & \bar{Q}_{22} & \bar{Q}_{26} \\ \bar{Q}_{16} & \bar{Q}_{26} & \bar{Q}_{66} \end{bmatrix}_j \left(\begin{Bmatrix} {\varepsilon^o}_x \\ {\varepsilon^o}_y \\ {\gamma^o}_{xy} \end{Bmatrix} (h_j - h_{j-1}) + \begin{Bmatrix} \kappa_x \\ \kappa_y \\ \kappa_{xy} \end{Bmatrix} \frac{1}{2} ({h_j}^2 - {h^2}_{j-1}) \right) \right\} \tag{3.15}$$

$$\begin{Bmatrix} M_x \\ M_y \\ M_{xy} \end{Bmatrix} = \sum_{j=1}^{N} \left\{ \begin{bmatrix} \bar{Q}_{11} & \bar{Q}_{12} & \bar{Q}_{16} \\ \bar{Q}_{12} & \bar{Q}_{22} & \bar{Q}_{26} \\ \bar{Q}_{16} & \bar{Q}_{26} & \bar{Q}_{66} \end{bmatrix}_j \left(\begin{Bmatrix} {\varepsilon^o}_x \\ {\varepsilon^o}_y \\ {\gamma^o}_{xy} \end{Bmatrix} (h_j - h_{j-1}) + \begin{Bmatrix} \kappa_x \\ \kappa_y \\ \kappa_{xy} \end{Bmatrix} \frac{1}{3} ({h_j}^3 - {h^3}_{j-1}) \right) \right\} \tag{3.16}$$

The force and bending moment resultants are finally given by Equations 3.17 and 3.18

$$\begin{bmatrix} N_x \\ N_y \\ N_{xy} \end{bmatrix} = [A] \begin{bmatrix} \varepsilon^o{}_x \\ \varepsilon^o{}_y \\ \gamma^o{}_{xy} \end{bmatrix} + [B] \begin{bmatrix} \kappa_x \\ \kappa_y \\ \kappa_{xy} \end{bmatrix} \tag{3.17}$$

$$\begin{bmatrix} M_x \\ M_y \\ M_{xy} \end{bmatrix} = [B] \begin{bmatrix} \varepsilon^o{}_x \\ \varepsilon^o{}_y \\ \gamma^o{}_{xy} \end{bmatrix} + [D] \begin{bmatrix} \kappa_x \\ \kappa_y \\ \kappa_{xy} \end{bmatrix} \tag{3.18}$$

Where N_x is normal force resultant in the x-direction, N_y is normal force resultant in the y-direction, N_{xy} is the inplane shear force resultant, M_x is bending moment resultant in the yz plane, M_y is bending moment resultant in the xz plane, and M_{xy} is twisting moment resultant. As mentioned earlier, all force and moment resultants are calculated per unit width.

Where $[A]$ is the Extensional stiffness matrix for laminate with dimensions of force/length and units of N/m is given as

$$[A] = \begin{bmatrix} A_{11} & A_{12} & A_{16} \\ A_{12} & A_{22} & A_{26} \\ A_{16} & A_{26} & A_{66} \end{bmatrix} \tag{3.19}$$

$[B]$ is the Bending-Extension coupling matrix for laminate with dimensions force×length/length and units in $Newtons$ is given as

$$[B] = \begin{bmatrix} B_{11} & B_{12} & B_{16} \\ B_{12} & B_{22} & B_{26} \\ B_{16} & B_{26} & B_{66} \end{bmatrix} \tag{3.20}$$

$[D]$ is the Bending-Curvature matrix for laminate with dimensions force×length and units in $N.m$ is given as

$$[D] = \begin{bmatrix} D_{11} & D_{12} & D_{16} \\ D_{12} & D_{22} & D_{26} \\ D_{16} & D_{26} & D_{66} \end{bmatrix} \tag{3.21}$$

From Equations 3.19-3.21 the normal forces and bending moments are given by

$$\begin{bmatrix} N_x \\ N_y \\ N_{xy} \end{bmatrix} = \begin{bmatrix} A_{11} & A_{12} & A_{16} \\ A_{12} & A_{22} & A_{26} \\ A_{16} & A_{26} & A_{66} \end{bmatrix} \begin{bmatrix} {\varepsilon^o}_x \\ {\varepsilon^o}_y \\ {\gamma^o}_{xy} \end{bmatrix} + \begin{bmatrix} B_{11} & B_{12} & B_{16} \\ B_{12} & B_{22} & B_{26} \\ B_{16} & B_{26} & B_{66} \end{bmatrix} \begin{bmatrix} \kappa_x \\ \kappa_y \\ \kappa_{xy} \end{bmatrix} \tag{3.22}$$

$$\begin{bmatrix} M_x \\ M_y \\ M_{xy} \end{bmatrix} = \begin{bmatrix} B_{11} & B_{12} & B_{16} \\ B_{12} & B_{22} & B_{26} \\ B_{16} & B_{26} & B_{66} \end{bmatrix} \begin{bmatrix} {\varepsilon^o}_x \\ {\varepsilon^o}_y \\ {\gamma^o}_{xy} \end{bmatrix} + \begin{bmatrix} D_{11} & D_{12} & D_{16} \\ D_{12} & D_{22} & D_{26} \\ D_{16} & D_{26} & D_{66} \end{bmatrix} \begin{bmatrix} \kappa_x \\ \kappa_y \\ \kappa_{xy} \end{bmatrix} \tag{3.23}$$

Where $[A]$, $[B]$, and $[D]$ elements are calculated as follows

$$A_{mn} = \sum_{j=1}^{N} [\overline{Q_{mn}}]_j \left(h_j - h_{j-1}\right) \tag{3.24}$$

$$B_{mn} = 1/2 \sum_{j=1}^{N} [\overline{Q_{mn}}]_j \left({h^2}_j - {h^2}_{j-1}\right) \tag{3.25}$$

$$D_{mn} = 1/3 \sum_{j=1}^{N} [\overline{Q_{mn}}]_j \left({h^3}_j - {h^3}_{j-1}\right) \tag{3.26}$$

Putting Equations 3.22 and 3.23 together in matrix form:

$$\begin{bmatrix} N_x \\ N_y \\ N_{xy} \\ M_x \\ M_y \\ M_{xy} \end{bmatrix} = \begin{bmatrix} A_{11} & A_{12} & A_{16} & B_{11} & B_{12} & B_{16} \\ A_{12} & A_{22} & A_{26} & B_{12} & B_{22} & B_{26} \\ A_{16} & A_{26} & A_{66} & B_{16} & B_{26} & B_{66} \\ B_{11} & B_{12} & B_{16} & D_{11} & D_{12} & D_{16} \\ B_{12} & B_{22} & B_{26} & D_{12} & D_{22} & D_{26} \\ B_{16} & B_{26} & B_{66} & D_{16} & D_{26} & D_{66} \end{bmatrix} \begin{bmatrix} {\varepsilon^o}_x \\ {\varepsilon^o}_y \\ {\gamma^o}_{xy} \\ \kappa_x \\ \kappa_y \\ \kappa_{xy} \end{bmatrix} \tag{3.27}$$

Putting 3.27 in compact form yields

$$\begin{bmatrix} N \\ - - \\ M \end{bmatrix} = \begin{bmatrix} A \mid B \\ - - - \\ B \mid D \end{bmatrix} \begin{bmatrix} \varepsilon^o \\ - - \\ \kappa \end{bmatrix} \tag{3.28}$$

The inverse of Equation 3.28 is

$$\begin{bmatrix} \varepsilon^o \\ - - \\ M \end{bmatrix} = \begin{bmatrix} A^* \mid B^* \\ - - - \\ B^* \mid D^* \end{bmatrix} \begin{bmatrix} N \\ - - \\ \kappa \end{bmatrix} \tag{3.29}$$

Where

$$[A^*] = [A]^{-1}$$

$$[B^*] = -[A]^{-1}[B]$$

$$[C^*] = [B][A]^{-1}$$

$$[D^*] = [D] - [B][A]^{-1}[B]$$

The matrices $[A], [B]\ and\ [D]$ correpond to extensional, bending-extension coupling and bending stiffness, respectively. Their terms possess physical meaning and provide a unique charactersitics in composites. Elastic tailoring of composites is a superior characteristic as its advantages exceed those of specific strength and specific stiffness (or weight saving

advantages of composites). One aim of elastic tailoring is to align the structure's optimal strength along the direction of critical loading. While the most important objective of elastic tailoring is to develop a smart structure able to adapt to load application providing enhanced performance. Elastic coupling and tailoring of laminate stiffness is not a standard practice and is not sought for all applications. As a matter of fact elastic coupling is not a necessary requirement for pressure vessels and consequently not required for risers. Therefore, elastic coupling is not addressed in this work.

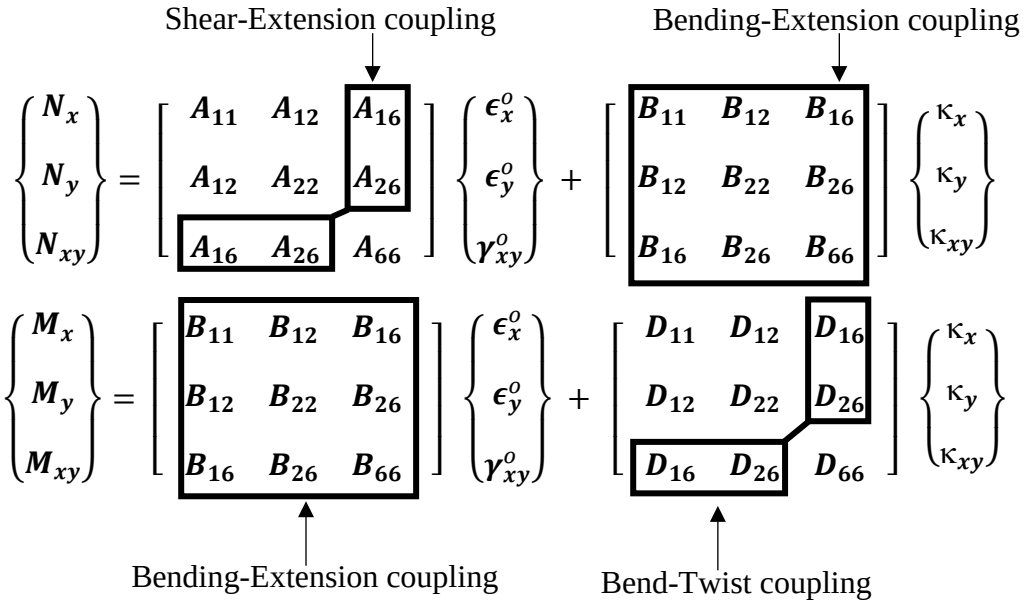

Design considerations

In order to eliminate elastic coupling in composite laminated structures, symmetric stacking sequence is followed. In this case highlighted elements of $[A], [B]\ and\ [D]$ corresponding to coupling stiffness will become trivial. For each ply above the midplane, there is an identical ply (in material, thickness, and fiber orientation angle) at an equal distance below the midplane. The following can be said of laminates that are symmetrical in both geometry and properties about the middle surface:

- Each lamina has the same thickness.
- Corresponding laminae based on their relative location from the midplane are of the same material properties and principal material orientations.
- For symmetrical laminate $[B] = 0$ → No Extension-Bending Coupling, and hence Equation 3.28 becomes:

$$\begin{bmatrix} N \\ -- \\ M \end{bmatrix} = \begin{bmatrix} A \mid 0 \\ --- \\ 0 \mid D \end{bmatrix} \begin{bmatrix} \varepsilon^0 \\ -- \\ \kappa \end{bmatrix} \tag{3.30}$$

In this study a symmetric laminae e.g.$[90/\quad \pm 45/\quad 0]_s$ is proposed as shown in Figure 3-7. This selection is mainly based on choosing a preferred stacking sequence which has specific properties. In this case, the $0°$ oriented layers resist the axially applied loads as well as bending then the $0°$ oriented layers together with ones oriented at $90°$ resist internal pressure. Finally, shear stresses developed in and out of-plane or the pipe are resisted using layers oriented at $\pm 45°$.

The proposed stacking sequence results in a quasi-isotropic laminate, which implies same elastic modulus at all directions in the plane of the laminate. In other words, the laminate is isotropic only in its plane.

For laminates with symmetric stacking sequence, the homogenization technique can lead to effective results. Mathematical homogenization enables expressing the effective inplane properties as explained in [19]. The physical meaning of homogenization is to estimate the material properties of the laminate 'as if' it were made of isotropic material. In other words, it is to answer the question "*assuming homogeneous isotropic material, what would be the mechanical properties used?*" The procedure and derivation of homogenized properties are provided in the next subsection.

Substituting in Equations 3.17 and 3.18 with $[B] = 0$, the midplane strains and curvatures equations become

$$\begin{bmatrix} \varepsilon_{xx}^{o} \\ \varepsilon_{yy}^{o} \\ \gamma_{xy}^{o} \end{bmatrix} = [A^{-1}] \begin{bmatrix} N_{xx} \\ N_{yy} \\ N_{xy} \end{bmatrix}$$

And

$$\begin{bmatrix} \kappa_{xx} \\ \kappa_{yy} \\ \kappa_{xy} \end{bmatrix} = [D^{-1}] \begin{bmatrix} M_{xx} \\ M_{yy} \\ M_{xy} \end{bmatrix}$$

In a symmetric laminate, in-plane forces cause only in-plane strains and no curvatures. Also, the bending and twisting moments cause only curvatures and no in-plane strains [19].

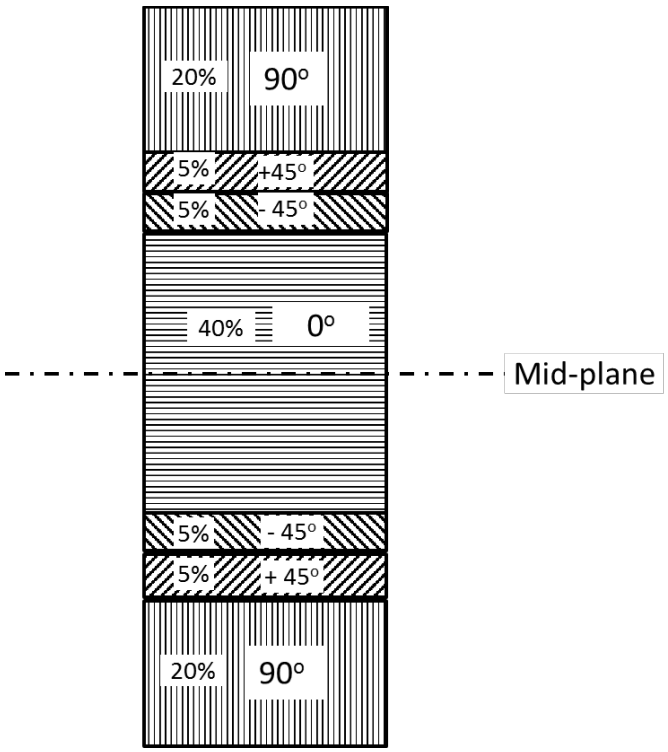

Figure 3-7: Proposed laminate layup configurations

Laminate Properties

This study focused on one of the preferred stacking sequences indicated earlier. The specific properties of this sequence are due to the 0° oriented layers resisting the axially applied loads as well as bending and that the 0° oriented layers together with ones oriented at 90° resist internal pressure. Additionally, shear stresses developed in and out of-plane or the pipe are resisted using layers oriented at $\pm 45°$. Given the highest priority of axial loading and internal pressure the laminate with stacking of $[90/\quad \pm 45/\quad 0]_s$ possess 40% of laminae are in 0° as well as 40% is in the 90° direction while the remaining 20% is in $\pm 45°$ directions. Table 3.1 and Figure 3-7 show the stacking sequence laminate

$[90/\ \pm 45/\ 0]_s$ with pile percent of its laminae. The sequence and pile percent help to find the composite materials' properties from design figures and tables shown in Appendix A.

Table 3.1: Stacking sequence laminate with pile percent

Pile Percent %	40%	20%	40%
Stacking angle	90°	$\pm 45°$	0°

The actual design of a composite structure practically starts with stacking sequence selection and corresponding pile percentage. For example based on a given diameter chosen based on required mass flow rate, a first step can be to select the suitable thickness then calculate the $A, B,$ and D matrices. Afterwards, based on applied loads the designer calculates strains ε and curvatures κ, and then calculates stresses σ in each lamina. Finally, the designer apply the failure criteria to predict potential of failure in any lamina. In case a lamina is predicted to fail or be close to failure the design is revisited to increase the number of laminates by increasing the thickness and/or change the stacking sequence and pile percentages. This process is repeated until no lamina is expected/predicted to fail. Figure 3-8 shows a flowchart for iterative design process based on failure prediction within laminae. It can be observed the design with composites is significantly different from design with metals, e.g. steel or aluminum. It can also be understood that this significant difference results in adding further ambiguity to the design process. Therefore, straight forward comparison between a composite pipeline and its metallic counterpart can be hindered due to lack of common basis for comparison. For this purpose composite homogenization techniques are developed to enable the designer to develop preliminary comparison basis with metals. In brief, homogenization techniques are used to enable treating composite structure "as if" they were

made of homogenous material. The next section provides overview of the homogenization technique in composites.

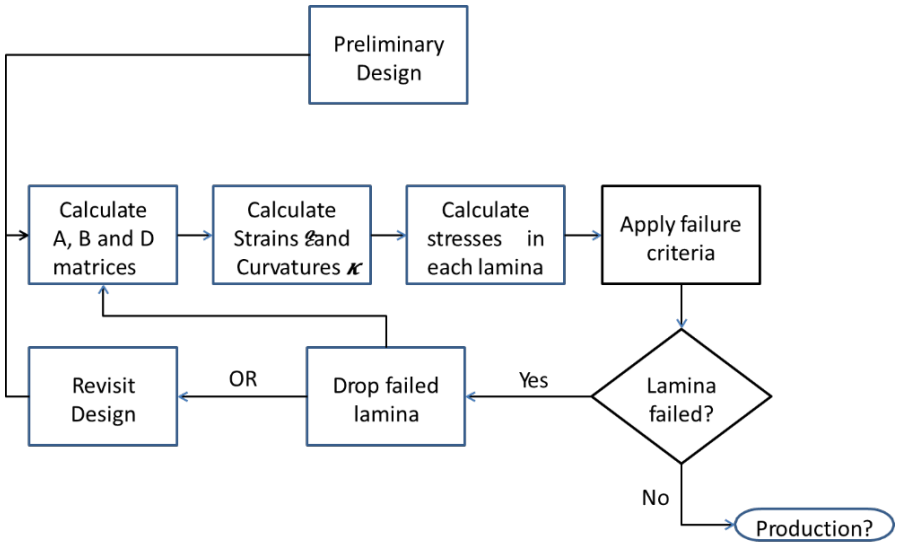

Figure 3-8: Failure prediction

3.2.3 Homogenization

A homogeneous material has the same properties at any point. In other words, properties do not depend on the location. Applying homogenization technique enables, obtaining equivalent or homogenized mechanical properties (such as E, ν, and G) and failure limits in tension and compression. In the following, the discussion and equations for homogenization are presented below and are based on the work in [19].

For the balanced symmetric laminate particular to proposed pipeline design, the extensional stiffness matrix is

$$[A] = \begin{bmatrix} A_{11} & A_{12} & 0 \\ A_{12} & A_{22} & 0 \\ 0 & 0 & A_{66} \end{bmatrix}$$

Where the coupling stiffness matrix $[B] = [0]$.

The inverse of the $[A]$ matrix is

$$[A^{-1}] = \frac{1}{A_{11}A_{22} - A_{12}^2} \begin{bmatrix} A_{22} & -A_{12} & 0 \\ -A_{12} & A_{11} & 0 \\ 0 & 0 & \frac{(A_{11}A_{22} - A_{12}^2)}{A_{66}} \end{bmatrix} \tag{3.31}$$

By inversing Equations 3.22 and 3.23, the strains and curvatures are given as

$$\begin{bmatrix} \varepsilon_{xx}^o \\ \varepsilon_{yy}^o \\ \gamma_{xy}^o \end{bmatrix} = [A_1] \begin{bmatrix} N_{xx} \\ N_{yy} \\ N_{xy} \end{bmatrix} + [B_1] \begin{bmatrix} M_{xx} \\ M_{yy} \\ M_{xy} \end{bmatrix}$$

$$\begin{bmatrix} \kappa_{xx} \\ \kappa_{yy} \\ \kappa_{xy} \end{bmatrix} = [C_1] \begin{bmatrix} N_{xx} \\ N_{yy} \\ N_{xy} \end{bmatrix} + [D_1] \begin{bmatrix} M_{xx} \\ M_{yy} \\ M_{xy} \end{bmatrix}$$

Where

$$[A_1] = [A^{-1}] + [A^{-1}][B][(D^*)^{-1}][B][A^{-1}]$$

$$[B_1] = -[A^{-1}][B][(D^*)^{-1}]$$

$$[C_1] = -[(D^*)^{-1}][B][A^{-1}] = [B_1]^T$$

$$[D^*] = [D] - [B][A^{-1}][B]$$

$$[D_1] = [(D^*)^{-1}]$$

For a symmetric laminate $[B] = [0]$, and therefore, $[A_1] = [A^{-1}]$, $[B] = [C_1] = [0]$ and $[D_1] = [D^{-1}]$. In this case the strains and curvatures equations for midplane become

$$\begin{bmatrix} \varepsilon_{xx}^{o} \\ \varepsilon_{yy}^{o} \\ \gamma_{xy}^{o} \end{bmatrix} = [A^{-1}] \begin{bmatrix} N_{xx} \\ N_{yy} \\ N_{xy} \end{bmatrix} \tag{3.32}$$

$$\begin{bmatrix} \kappa_{xx} \\ \kappa_{yy} \\ \kappa_{xy} \end{bmatrix} = [D^{-1}] \begin{bmatrix} M_{xx} \\ M_{yy} \\ M_{xy} \end{bmatrix} \tag{3.33}$$

Substituting Equation 3.31 into Equation 3.32 yields

$$\begin{bmatrix} \varepsilon_{xx}^{o} \\ \varepsilon_{yy}^{o} \\ \gamma_{xy}^{o} \end{bmatrix} = \frac{1}{A_{11}A_{22} - A_{12}^2} \begin{bmatrix} A_{22} & -A_{12} & 0 \\ -A_{12} & A_{11} & 0 \\ 0 & 0 & \frac{(A_{11}A_{22} - A_{12}^2)}{A_{66}} \end{bmatrix} \begin{bmatrix} N_{xx} \\ N_{yy} \\ N_{xy} \end{bmatrix} \tag{3.34}$$

Assuming that the laminate is subjected to a uniaxial tensile stress σ_{xx} in the x-direction with σ_{yy} , τ_{xy} are zero. For h is the laminate thickness then the tensile and shear forces per unit width in the xy plane can be expressed as $N_{xx} = h\sigma_{xx}$, $N_{yy} = 0$ and $N_{xy} = 0$ substituting in Equation 3.34 then we obtain

$$\varepsilon_{xx}^{o} = \frac{A_{22}}{A_{11}A_{22} - A_{12}^2} h\sigma_{xx},$$

$$\varepsilon_{yy}^{o} = -\frac{A_{12}}{A_{11}A_{22} - A_{12}^2} h\sigma_{xx},$$

$$\gamma_{xy}^{o} = 0$$

Based on these strains the homogenized modulus and Poisson's ratio can be obtained as

$$E_{xx} = \frac{\sigma_{xx}}{\varepsilon^o_{xx}} = \frac{A_{11}A_{22} - A_{12}^2}{hA_{22}}, \tag{3.35}$$

$$v_{xy} = -\frac{\varepsilon^o_{yy}}{\varepsilon^o_{xx}} = \frac{A_{12}}{A_{22}}, \tag{3.36}$$

In turn, applying N_{yy} and N_{xy} separately, we can find

$$E_{yy} = \frac{A_{11}A_{22} - A_{12}^2}{hA_{11}},$$

$$v_{yx} = \frac{A_{12}}{A_{11}}$$

$$G_{yx} = \frac{A_{66}}{h} \tag{3.37}$$

Applying the discussed procedures to proposed design must start from the mechanical properties of a unidirectional layer. These nominal properties are provided in Table 3.2. These properties are used to calculate the reduced stiffness matrix $\bar{Q}$ at general orientation.

Table 3.2: Nominal values of Carbon/Epoxy [32]

Properties	Carbon/Epoxy
Longitudinal elastic modulus E_l (GPa)	134
Transverse elastic modulus E_t (GPa)	7
Shear modulus $G_{lt}(GPa)$	4.2
Poisson Ratio v_{lt}	0.25

In other words the dataset shown in Table 3.2 is used to calculate the reduced stiffness matrix based, then using Equation 3.24 to calculate the value of A, and applying it on the proposed stacking shown in Table 3.1.

$$A_{mn} = (0.4\,\bar{Q}_{mn_{90^\circ}} + 0.4\,\bar{Q}_{mn_{0^\circ}} + 0.1\,\bar{Q}_{mn_{45^\circ}} + 0.1\bar{Q}_{mn_{-45^\circ}}) \times t$$

where t is the stacking laminate thickness.

Equations 3.35, 3.36, and 3.37, are used to calculate the homogenized properties, i.e. E_{xx} , ν_{xy} , G_{xy} as shown in Table 3.3.

Table 3.3: The calculated properties of the proposed stacking laminate

Property	The proposed stacking laminate $[90/\ \pm 45/\ 0]_s$
Longitudinal Young Modulus E_{xx} (GPa)	63.7621
Shear Modulus G_{xy} (GPa)	10.258
Poisson Ratio ν_{xy}	0.1186

Similar to the procedure used to obtain homogenized material properties, failure limits in tension and compression are calculated and provided in Table 3.5 in section 3.3 together with other mechanical and thermal properties calculated. All homogenized properties and failure limits calculated within are consistent with design charts provided in Appendix A and obtained from [32].

To this end all design methods and practices used for homogenous isotropic metals can be applied to the proposed composite design. It must be noted this process is developed to

enable preliminary comparisons. Meanwhile, for final design optimization and refinement, composite materials offer myriads of options to develop a much superior structure when compared to metallic counterpart.

Isotropic

For isotropic materials, properties do not depend on orientation and the shear strength is equal in all directions [19]. The outcome of homogenization enabled treating the proposed symmetrically stacked composite as an isotropic material in which: $E_1 = E_2 = E$, $\nu_{12} = \nu_{13} = \nu_{23} = \nu$, and $G_{12} = G_{13} = G$. For the isotropic material in plane stress ($\sigma_{zz} = \tau_{xz} = \tau_{yz} = 0$).

$$\begin{bmatrix} \varepsilon_{xx} \\ \varepsilon_{yy} \\ \varepsilon_{xy} \end{bmatrix} = \begin{bmatrix} \frac{1}{E} & -\frac{\nu}{E} & 0 \\ -\frac{\nu}{E} & \frac{1}{E} & 0 \\ 0 & 0 & \frac{1}{G} \end{bmatrix} \begin{bmatrix} \sigma_{xx} \\ \sigma_{yy} \\ \tau_{xy} \end{bmatrix} \tag{3.38}$$

3.2.4 Simplified Analyses

Applied assumptions in terms of plane stress and homogenization of materials are essential for this section. It must be understood these assumptions are valid mainly within the linear regime. Stress-strain behavior of carbon fibres composites is dominated by linear behavior displaying minimal plastic zone till failure. Therefore simplified analyses using Euler Theories [30] are suited for axial, bending, and buckling behavior. In this context, and based on actual geometry of the laminated composite pipeline.

Euler-Bernoulli Beam Theory

The Euler-Bernoulli (E-B) beam theory utilizes three major of concepts, namely:

- Continuum: for any point ‘p’ in a beam, all points were in its vicinity before deformation remain in the vicinity of the same point after deformation.
- Homogenous isotropic material.
- Small strain (linear theory): This is the most important assumption for linear theories.

It can be seen that all these concepts are guaranteed and in particular isotropy once homogenization is attained. In the meantime, continuum concept is valid for composites as well as small strain assumption without conservation.

Restrictions

Restrictions can be simply explained as the operation conditions of the structure under study. These are based on applied load and the particular geometry of the structure. A sufficient conditions on geometry of the structure is to possess length-to-depth ratio greater than 10 and for a pipeline to have at least the same ratio between diameter and wall thickness.

1. Slender bar (cross-sectional dimensions $\ll$ length).
2. Uniform and symmetric cross-section.
3. Uniform (constant) bending moment.

Restriction on uniformity of applied load is not as stringent as the ones imposed on geometry. In other words, accurate results due to nonuniform bending moment can be obtained as long as slenderness is maintained.

Assumptions

All assumptions are made to enable developing the Euler Bernoulli beam theory. They are all imposed on the cross-section. All these are valid in the case of a composite pipeline.

1. Plane cross-section remains plane.
2. Normal cross-section remains normal.
3. Rigid cross-section.

Therefore, based on the above restrictions and assumptions different types of stresses can be calculated based on external applied loads on the pipeline. With the assumption on linearity being made, superposition also becomes valid. In superposition, the stresses developed due to individual loads can be examined independently. For example, normal stress is developed in a beam (or a pipeline) due to axial load, bending and internal pressure

The normal stress due to axial load, F is defined as

$$\sigma = \frac{F}{A} \tag{3.39}$$

Where is σ the normal stress (N/m^2), F the axial force (N) and A the cross-sectional area (m^2).

While the normal stress due to bending moment is defined as follows

$$\sigma = -\frac{M}{I}y \tag{3.40}$$

Where σ is the normal stress (N/m^2) , M is the bending moment in $(N.m)$, y is the perpendicular distance from the neutral axis in (m) and I is the second moment of area of cross-section in (m^4).

As for analyzing stresses in the pipeline due to internal pressure can be enabled using plane stress analysis of pressure vessel. An independent section is dedicated for this situation as internal pressures result in both normal and shear stresses.

Another essential scenario must be considered is the potential of buckling of a pipeline under axial loads. The high slenderness ratio of a pipeline enables using Euler theory for buckling which is based on linear approximation of curvature. One of the requirements for this theory is to use a homogenized Young' modulus for the material. Assuming steel versus composite pipeline possessing identical geometry and boundary conditions the Euler critical load can be calculated. At this critical value the out-of-plane deformations (normal to axial direction) become highly noticed. It is to be understood that buckling is not a failure mode, instead it defines the loss of carrying capacity in the axial direction.

Therefore, for composite and metallic pipelines alike the Euler critical load is defined as follows

$$P_E = \left(\frac{\pi}{L}\right)^2 EI \tag{3.41}$$

Where P_E is the Euler critical load (N), E is the modulus of elasticity (Pa) of the pipeline material, I is the second moment of area of the pipeline cross section (m^4) and L is the length of the pipeline.

3.3 Comparisons

The design requirements of pipelines include geometric ones such as thickness and diameter as well as material specific ones such as thermal characteristics, weight, strength,

failure limit, cost, etc. All these can be attained for certain design based on internal/external loading conditions for different types of loading. Whereas the design constraints may be imposed on a subset of these requirements such as strength, failure limit or cost. In this work a major focus is paid towards flow assurance. Therefore, thermal characteristics of the material used for the pipeline is of essential importance. Consequently, to provide a fair comparison a number of geometric parameters are to be maintained common between steel versus composite pipeline. For example, identical length pipelines are used given that the length is constrained by the physical location of the drilling/production site. Similarly, the pipeline diameter controls the mass flow rate which is a requirement of production. Moreover, for meaningful comparison identical thickness pipelines (steel vs. composite) are to be considered. This is based on the study presented in the previous chapter in which same thickness pipelines were studied to compare their abilities to provide enhanced thermal characteristics.

Comparison in terms of weight, internal load, stresses, failure, corrosion, and cost of the SCR and CCR are conducted using the dataset presented in Table 3.4. This data set was collected from the Asgard Flowlines Project [6] to guarantee comparisons of a practical solutions.

Table 3.4: Dataset of the Asgard flowlines project

Pipeline outer Diameter D_O, m	0.2518
Pipeline wall thickness t, m	0.0116
Design Pressure P, bar	350

Moreover, this section also conducts a comparison between steel and composite for other mechanical properties. The dataset is shown in (Table 3.5) where the data for the steel is taken from [31] and the data for the Carbon/Epoxy is taken from [32].

Table 3.5: Mechanical properties for steel versus composite as taken from [31] and [32]

Mechanical Properties	Steel	Carbon/Epoxy $[90/\pm45/\ 0]_s$
Young's Modules E, GPa	210	63.729
Shear Modules G, GPa	78	10.257
Poisson ratio ν	0.3	0.12
Max. Tensile stress MPa	500	391
Max. Compression stress MPa	500	537
Max. Shear stress MPa	250	118
Coefficient of Thermal expansion α $(°C^{-1})$	0.1×10^{-5}	0.05×10^{-5}

3.3.1 Weight Calculation

One of the most significant advantages of composite materials over metals is their low density and light weight. This is one of the substantial reasons for designers to switch from SCR to CCR. The proposed usage of CCR will contribute towards reducing the size of tensioners for the tension requirement (alleviating buckling under own weight) hence the size and weight of the platform; i.e. the whole system weight [21-23].

According to [6], the pipe weight per unit length W_P is calculated as follows:

$$W_P = \frac{\pi \rho g}{4} \left({D_o}^2 - {D_i}^2 \right) \tag{3.42}$$

Where ρ is pipeline density, D_o is pipe outer diameter, D_i is pipe inner diameter.

For steel pipelines, the weight per unit length is defined as

$$W_s = \frac{\pi}{4}\gamma_s\,({D_o}^2 - {D_i}^2) \tag{3.43}$$

Where γ_s is the steel specific weight.

Whereas, for the composite pipelines, the weight per unit length is defined as

$$W_c = \frac{\pi}{4}\gamma_c\,({D_o}^2 - {D_i}^2) \tag{3.44}$$

Where γ_c is the composite specific weight.

By dividing Equation 3.43 by Equation 3.44, the weight ratio between steel and composite is calculated using Equation 3.45. The data used in calculating the ratio (γ_s and γ_c) are based on Table 3.5.

$$\frac{W_s}{W_c} = \frac{\gamma_s}{\gamma_c} \tag{3.45}$$

Table 3.6: Specific weight of composite and steel [33]

	Specific Weight kN/m^3
Steel (γ_s)	76.52
Composite (γ_c)	15.7

The resulting ratio between steel and composite is found to be

$$\frac{W_s}{W_c} = 4.874$$

Also, the data from Tables 3.4 and 3.6 are used in Equations 3.43 and 3.44 to calculate the weight per unit length for steel and composite as shown in Table 3.7.

Table 3.7 Results of weight per unit length for steel and composite

	Weight per unit length (N/m)
Steel	669.82
Composite	137.43

Table 3.7 and the result of the ratio between steel and composite prove that the steel is almost 5 times heavier than composite. This has implications on the size of the platform, the whole system weight, and the tension requirement load.

3.3.2 Pressure

The internal pressure generates internal stresses within the walls of the pipeline. The pipeline can be idealized as a cylindrical pressure vessel as shown in Figure 3-9 where the biaxial normal stress state is provided by Equation 3.46.

$$\sigma_1 = \frac{Pr}{t}, \qquad \sigma_2 = \frac{Pr}{2t} \tag{3.46}$$

Considering the high ratio between pipeline diameter and its thickness (Table 3.4, $D_o/t = 21.7$) plane stress assumptions can be utilized. In this case stresses normal to the thickness, i.e. σ_3, are assumed negligible or zero as shown in Figure 3-9. Therefore, in order to calculate the inplane shear stress within the pipeline walls Mohr's circle can be used as shown in Figure 3-10. In this case $\tau_{max} = \sigma_1/2 = \sigma_2$, i.e. based on Tresca failure criterion. It must be noted that shear stresses are significant in terms of causing failure in all ductile materials. Meanwhile, composites are much weaker in resisting shear stresses. A designer

may approach the problem with extreme caution simply because a pressurized pipeline "bursts" mainly due to shear stresses.

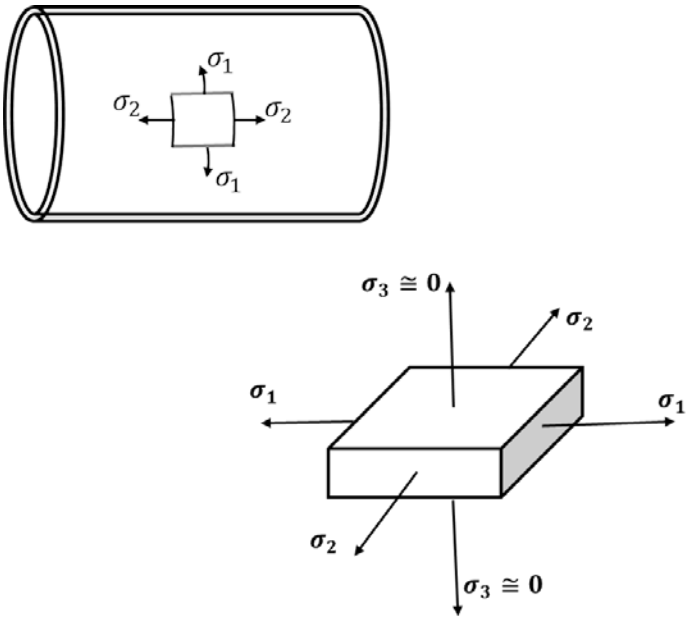

Figure 3-9: Wall stresses in a pipeline section

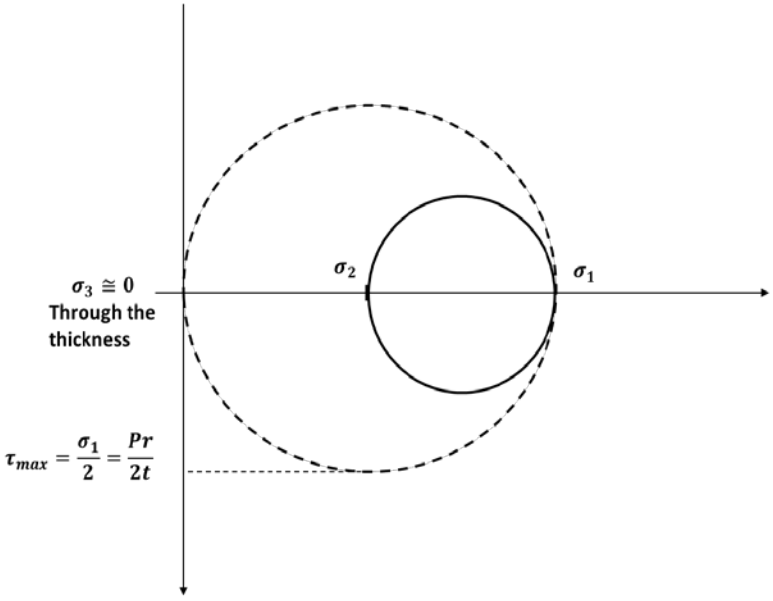

Figure 3-10: Mohr's Circle

After the principle stresses are calculated using Equation 3.46, Mohr's Circle (shown in Figure 3-10) can be used to calculate the maximum shear stress.

To compare the shear stresses for the steel and carbon/epoxy pipelines, the dataset presented in Table 3.4 is used. This data set was collected from the Asgard Flowlines Project [6]. From the data of the Asgard flowlines in Table 3.4, the ratio ${D_o}/{t}$ is calculated as

$$ {D_o}/{t} = 21.7 $$

The calculated value of ${D_o}/{t}$ confirms the validity of the assumption that the thickness is 10 times less than pipeline radius (${r}/{t} > 10 \quad or \quad {D}/{t} > 20$).

The ratio of internal pressures based on normal stresses is equal to the ratio between maximum tensile strength of different materials

$$ {p_s}/{p_c}\big|_{Normal} = {500}/{391} = 1.28 $$

Meanwhile, the ratio of internal pressure based on maximum sear strength is

$$ {p_s}/{p_c}\big|_{Normal} = {250}/{118} = 2.12 $$

Therefore, it is clear that shear stresses must be used by the designer to establish meaning comparison. It is also logical and realistic as ductile materials as steel would fail due to shear while composite materials are much weaker in shear than tension or compression.

Using the data in Table 3.4, the shear stress in the Asgard data set is calculated as follows:

$$ \tau_{Asgard} = \frac{Pr}{2t} = \frac{PD_o}{4t} \tag{3.47} $$

$$\tau_{Asgard} = 189.94\ MPa$$

Steel being ductile will fail due to shear as shown in Table 3.5.

$$\tau_{max} = 250MPa$$

The Factor of Safety (FoS) for steel and composite (Carbon/Epoxy) is

$$FoS = \frac{\tau_{max}}{\tau_{Asgard}}$$

$$FoS_{steel} = \frac{250}{189.94} = 1.32$$

$$FoS_{Carbon/Epoxy} = \frac{118}{189.94} = 0.62$$

It is clear that the shear stress in the Asgard data set does not exceed allowable values for steel. A steel pipeline is much safer than C/E by comparing their corresponding factors of safety. Based on shear strength (being critical), the maximum pressure a steel pipeline can withstand is $23.034\ MPa$ while a composite pipeline withstands $10.87\ MPa$. However, the designer of composite pipelines would use a thicker pipeline to increase their factor of safety. This is mainly enabled by the fact that a C/E pipeline is 5-times lighter than its steel counterpart. Also a more advantageous aspect is that thicker C/E pipeline has the advantage of providing much better thermal insulation, resulting in better flow assurance.

Axial Stress

The following assumptions are considered in the comparison between SCR and CCR. Both pipeline materials are homogenous. The reason for this assumption is to be able to delineate factors associated with differences in strength and failure characteristics. Assuming

pipes to possess identical geometry as shown in Table 3.4 implies imposing the design constraints identified in thermal analysis in the previous chapter. It also entails the applicability of identical external loads, e.g. ocean current. Meanwhile the assumption of homogeneous materials allows for performing simplified analyses to delineate comparison objectives.

The normal stress due to axial load (F) is defined as follows (Equation 3.39 is repeated for convenience)

$$\sigma = \frac{F}{A} \tag{3.48}$$

Where σ the normal stress, F is axial force, A is the cross-sectional area.

Thus, the normal stress in the steel pipeline is defined as follows

$$\sigma_s = \frac{F_s}{A_s} \tag{3.49}$$

And the normal stress in the composite pipeline is defined as follows

$$\sigma_c = \frac{F_c}{A_c} \tag{3.50}$$

Since it is assumed that the two pipes have the same diameter and the same thickness: A_s=A_c.

Dividing Equation 3.49 by Equation 3.50 yields

$$\sigma_s/\sigma_c = F_s/F_c \tag{3.51}$$

The data from Tables 3.5 are used in Equations 3.52 to calculate the pipelines tension load carrying capacity as follows:

- Steel tension load carrying capacity calculation

$$F_{s_{max}} = \sigma_{all} * A_s \qquad (3.52 - A)$$

$$F_{s_{max}} = \ 4.588 * 10^6 \ N$$

- Composite tension load carrying capacity calculation

$$F_{c_{max}} = \sigma_{all} * A_c \qquad (3.52 - B)$$

$$F_{C_{max}} = 3.588 * 10^6 \ N$$

The results in Equations 3.52 which show the reduced pipeline capacity in the case of composite compared to the steel pipeline capacity in tension. Meanwhile these results are misleading and can be explained by revisiting Equations 3.51 in which the left hand side of the equation can be replaced by the tensile and compressive strength of steel versus carbon/epoxy pipeline materials. In the case of tension

$$F_s/F_c\Big|_{Tension} = 500/391 = 1.28$$

While in the case of compressive load

$$F_s/F_c\Big|_{Compress} = 500/537 = 0.93$$

This implies that Carbon/Epoxy is worse than steel in carrying tensile loads while C/E is better than steel for carrying compressive load. An oil riser is always under compressive

loads under its own weight. Therefore it is better to utilize composite pipeline, i.e. carbon epoxy pipeline.

3.3.3 Bending

Normal stresses due to bending based on Euler Bernoulli is provided in Equation 3.40 and repeated in Equation 3.53 for convenience

$$\sigma = -\frac{M}{I}y \tag{3.53}$$

Where σ is the normal stress due to bending (N/m^2) , M is the bending moment of neutral axis $(N.m)$, y is the perpendicular distance to neutral axis in (m) and I is the second moment of area of the cross-section in (m^4).

This thesis used the data in Tables 3.4 and 3.5 to calculate M, the moment of neutral axis, in steel pipelines. The steps of the calculations are detailed below.

Bending in Steel and Composite Pipelines

Using the data in Table 3.4, the tensile stress in the Asgard data set is calculated as follows. A property of steel is that the maximum tensile stress is the same as maximum compression Table 3.5; i.e. $500\ MPa$. Meanwhile for Carbon/Epoxy the tensile strength is $391\ MPa$ and the compressive strength is $537\ MPa$. Given identical geometry for steel and carbon pipeline the ratio of their moment carrying capacity can be calculated using Equation 3.53 as

$$\sigma_s/\sigma_c\big|_{Tension} = M_s/M_c\big|_{Tension} \tag{3.54}$$

Similarly, in compression

$$\sigma_s/\sigma_c\big|_{Compress} = M_s/M_c\big|_{Compress} \tag{3.55}$$

Therefore, the moment carrying capacity ratio between steel and composite in tension is 1.28 and in compression is 0.391. Given the symmetry of the cross-section (hollow circular) the critical ratio is the one associated to the tension side. Therefore, steel is considered a better material for the pipeline with ability to support 28% higher bending moment. Meanwhile, it is to remind the reader that a steel pipeline is 5 times the weight of its composite counterpart. Therefore, designing a heavier (thicker) composite pipeline with higher moment carrying capacity should represent no challenge. However, a thicker composite pipeline would further enhance flow assurance characteristics as mentioned earlier.

3.3.4 Buckling

Euler critical buckling theory is used to analyze the buckling resistance in the pipelines as follows

$$P_E = \left(\frac{\pi}{L}\right)^2 EI \tag{3.56}$$

Where P_E is the Euler critical load (N), E is the modulus of elasticity (Pa) of the pipeline material, I is the second moment of area of the pipeline cross section (m^4) and L is the length of pipeline.

The data from Table 3.5 will be used to calculate the buckling in case of steel and composite as shown below. Meanwhile given the identical geometry of pipelines an easier approach is to compare the ratio of their critical loads.

Critical Load ratio

Accounting for steel and composite pipelines of the same cross section ($I_s = I_c$) and same length the critical load ratio is

$$P_{E_s}/P_{E_c} = E_s/E_c = 3.3 \tag{3.57}$$

This indicates that a composite pipeline will buckle at one third of the load value of its steel counterpart. Therefore, a steel pipeline is considered better. Meanwhile the same critical load is desired for the composite pipeline can be guaranteed by imposing the condition $I_C \cong 3 \times I_S$. In other words, a thicker cross-section enables higher critical load value. An approximate expression for the second moment of area is

$$I \cong 4\pi r^3 t \tag{3.58}$$

For r is the mean radius of the pipeline and t is its thickness. Inspecting Equation 3.58, the designer realizes that increasing the thickness 3 times or increase of 0.45% in the radius allows tripling the composite pipeline to attain identical critical load capacity as the steel counterpart. A combination of increasing the radius and the thickness represents a better solution. Meanwhile, for a change in the pipeline radius the required mass flow rate must be considered. It should be noted that the restriction on maximum value of pipeline radius is imposed by the weight rather than the flow rate.

3.3.5 Corrosion and Cost

Two important factors are considered by designers when they select materials for pipelines: cost and corrosion resistance. Using materials with high corrosion resistance will reduce the cost for the whole life cycle of the pipeline.

One of the disadvantages of SCR is its poor corrosion resistance; the designers always need to consider both internal and external layers of anticorrosion. The internal surface of SCR is rougher than CCR, and also its surface finish will degrade and become rougher over time due to corrosion and/or scale buildup. Comparatively, the initial cost of CCR is higher than SCR. Saad et al. [21] reports a comparison of steel and composite cost, where the cost of steel is \$88.392/m and the cost of composite is \$116.4336/m. Hence, the cost factor between composite and steel is found to be 1.32.

Without a doubt a more detailed cost analysis is required to provide thorough comparison. Meanwhile the subject of cost analysis of composites is outside the scope of this work. Moreover, cost analysis of composites entails detailed procedures that always resulted in independent studies [34].

Comparisons between CCR and SCR should be based on the total life cycle cost that consider the initial capital costs and the operating and maintenance costs over the life of the pipeline. Hence, if designers consider the total life cycle cost (include operating and maintenance), SCR will be much more expensive than CCR. Moreover, CCR is lighter, which has implications on the size of the platform, the whole system weight, and the tension requirement load.

3.3.6 Summary of Comparison

In this subsection a more thorough approach is presented. It is always stated that composites have better "specific" properties when compared to metals. Therefore all earlier calculations are repeated then divided by the density of material used. Based on the previous sections to calculate the different properties of steel and composite, Table 3.8 provides the summarized of specific carrying capacities (i.e. dividing by density). Where density of steel and composite can be extracted from Table 3.6 to be $7800\ kg/m^3$ and $1600\ kg/m^3$, respectively.

Table 3.8: Steel versus composite

Properties	Steel	Carbon/Epoxy	$\mathcal{R}$
Weight per unit length (N/m)	669.82	137.43	--
Internal pressure per density ($Pa/kg.m^{-3}$)	2,953.07	6,793.75	2.3
Force per density in tension ($N/kg.m^{-3}$)	588.2	2242.5	3.8
Force per density in compression ($N/kg.m^{-3}$)	588.2	3079.38	5.2
Moment per density in tension ($N.m/kg.m^{-3}$)	32.22	122.82	3.8
Moment per density in compression ($N.m/kg.m^{-3}$)	32.22	168.69	5.2
Buckling per length per density ($N\ per\ unit\ length/kg.m^{-3}$)	16,814.10	24,874.37	1.5

Examining the third column in Table 3.8 provides the ratio $\mathcal{R}$ between composite and steel for a particular load carrying capacity. Therefore, it is clear from the comparison provided in the table that carbon epoxy pipeline is superior to the steel one. This advantage is revealed by calculating the carrying capacity per density of the material.

Also, to compare the overall heat transfer coefficient (OHTC) and the second moment of area ‘I’ (the mechanical property dominating mechanical stiffness) versus the wall thickness, Figures 3.11 and 3.12 are presented below. It can be clearly seen in both figures that increasing the thickness enhances flow assurance by exponentially reducing heat transfer coefficient and in the same increasing mechanical stiffness; both are favorable. Therefore, wall thickness proved to be the most dominant parameter of the design.

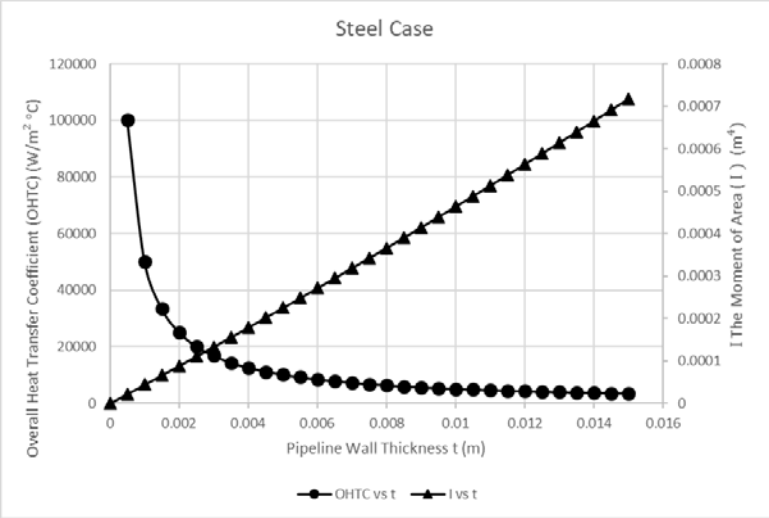

Figure 3-11: Comparison of OHTC and I versus the wall thickness in case of Steel

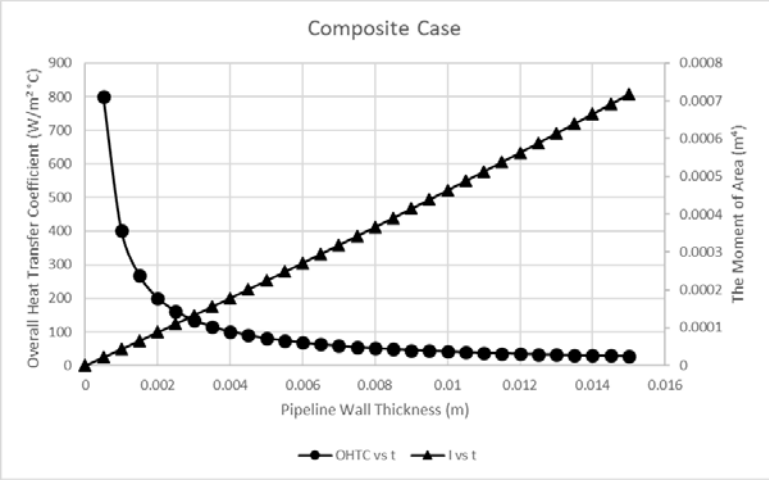

Figure 3-12: Comparison of OHTC and I versus the wall thickness in case of Composites

3.4 Conclusion

This chapter introduced in-depth details regarding the mechanics of composites, summarized in the Classical Lamination Theory. Later a brief discussion on the design of composite materials is used to clarify the challenge posed by different design techniques used for composites in comparison to methods used for metallic structures. Consequently, composites homogenization technique is discussed to alleviate this challenge and provide meaningful comparisons. Accordingly, an efficient comparison technique is proposed using simplified analyses addressing aspects related to particular failure mechanisms in ductile metals and composites. Simplified analyses enabled detailed comparisons of load carrying capacity in terms of internal pressure, axial load, bending moment and critical buckling load. It worth noting that simplified analyses are conservative when compared to CLT in the general sense. Meanwhile to establish the final design, detailed analysis using CLT and finite element analysis must be conducted. Finally, the specific load carrying capacities are utilizing the respective density of materials.

Table 3.8 provides overview comparison based on considerations discussed in section 3.3. The comparison indicates the comparative qualities and challenges associated to both steel and composite design. Further challenges for steel are associated with its corrosion and degradation in harsh environment. While composite corrosion may be less severe, their vulnerability to moisture absorption poses concerns regarding their degradation in this environment.

Published work in literature reflects a debate between two opinions, namely, one promotes steel and the other promotes composite. Researchers supportive of one opinion or the

other based their comparisons on solely thermal characteristics or crude mechanical properties. Therefore, in this chapter utilizing simplified analysis based on sound basis of homogenization enabled efficient comparisons. These comparisons indicated the potential of composite to be competitive to steel as a building material. The final and major conclusion can be based on the ratio of load carrying capacity, $\mathcal{R}$, between carbon/epoxy and steel which is always greater than 'one' in different loading scenarios. Therefore, it is proven that carbon/epoxy is an excellent candidate. Consequently, engineering should investigate detailed design of composite risers due to their benefits in being lightweight and corrosion resistant. These benefits when added to conclusions obtained from chapter 2 regarding their thermal characteristics form essential motive for considering them as excellent competitors to steels.

Chapter 4: Conclusions and Recommendation

This chapter presents the thesis summary and conclusions. It also discusses the limitations of the proposed methods. Finally, this chapter present recommendations and future directions.

4.1 Summary and Conclusions

This thesis focuses on guaranteeing flow assurance using thermal design-based methods. The thesis also focuses on the pipeline material itself to make sure that the temperature at any point in the pipeline is always above the solid deposit formation temperature, still in a feasibly economical manner. The proper selection of the pipeline material and its design parameters, such as the diameter and the thickness will prevent many of the problems associated with flow assurance.

To achieve the above overarching goals, the thesis quantitatively compares two solutions, an analytical solution and an approximate one, in terms of the thermal characteristics, and compares the output temperature profiles produced by these two solutions. This comparison is conducted in the steady state flow and on crud running inside steel pipelines with no insulations. Four case studies are examined based on varying the length of the steel pipeline and the flow rate of crud inside the pipeline. The results propose that the analytical solution is more accurate and can be generalized to different situations with varying lengths and flowrates.

Afterwards, this thesis studies and compares the thermal characteristics of traditional Steel Catenary Risers (SCR) and Composite Catenary Risers (CCR) to show which material

will keep the temperature above the solid deposit formation temperature. As predicted, the obtained results show that composite risers have enhanced thermal characteristics over its counterpart steel pipelines. However, many researchers and professionals from the industry will argue that the CCR have a higher cost, which hinders its economical deployment; therefore, other aspects of the performance must be considered. Performance aspects regarding material strength, expected life and minimal weight design constitute the most essential minimal set for these comparisons.

Overall, based on comprehensive investigations of the thermal characteristics, material strength, expected life, and minimal weight design, it was concluded that CCR provide a better design option for long-term operations.

4.2 Research Contribution

The main contribution of this research can be summarized as follows:

- A comparison of two prediction models to predict the temperature profile in the steady state flow based on: 1) An analytical solution, and 2) An approximate solution. The implementation is done using Matlab.
- A comparison of the temperature profile in steel pipelines and composite pipelines using the analytical solution.
- A comparison of steel and composite pipelines in terms of other design parameters, such as weight, bending, strength, corrosion, and cost.

4.3 Thesis Limitations

- The recommendation that CCR is a better design solution than traditional SCR is based on performance calculations that assume:
    - Long term operations to justify the initial high cost of CCR.
    - Pipelines have no insulation.
- For both steel and composite, nominal homogenized mechanical and heat transfer properties are used.
- Steel and composite pipeline have the same dimensions (the same diameter and the same thickness).
- The comparisons are made in the steady state flow only. No analysis was conducted in the transient state.

4.4 Future Work

The future work of this research will include extending the comparisons to be done in the transient state flow on top of the steady state flow presented in this thesis. Moreover, the study in this thesis assumed no insulations to be used on the pipelines. The future work will examine the effect of adding different insulation materials with different thicknesses on both steel and composite pipelines.

Finally, the results presented in this thesis are all based on simulations and computer programs. It is very useful to conduct a real experiment with real pipelines and measure the temperature inside them over time to validate the simulation results. The marine ocean tank at Memorial University can be used to immerse the pipelines inside it to act as the ocean environment that exists in real life.

References

1. Braestrup, M.W., et al., *Design and installation of marine pipelines*. 2005: Fairfield, NJ: ASME Press, Blackwell Publishing.
2. Audubon-Inc., *Basics of Subsea Pipeline Engineering*, *https://audubooncompanies.com/basics-of-subsea-pipeline-engineering/*. 2015.
3. Denniel, S., J. Perrin, and A. elix-Henry, *Review of Flow Assurance Solutions for Deepwater Fields.* Offshore Technology Conference. doi:10.4043/16686-MS, 2004.
4. Ellison, B.T., et al., *The Physical Chemistry of Wax, Hydrates, and Asphaltene*. Offshore Technology Conference. doi:10.4043/11963-MS, 2000.
5. BauckIrmann-Jacobsen, T., *Flow Assurance - A System Perspective.* University of Oslo, 2015.
6. Bai, Y. and Q. Bai, *Subsea Pipelines and Risers*. 2005: Elsevier Science.
7. CAPP, *Use of Reinforced Composite Pipe (Non-Metallic Pipelines).* The Canadian Association of Petroleum Producers (CAPP), 2017.
8. Bahadori, A., *Thermal Insulation Handbook for the Oil, Gas, and Petrochemical Industries*, *https://doi.org/10.1016/C2013-0-13424-1*. 2014: Gulf Professional Publishing.
9. Su, J., D. Cerqueira, and S.-Z. Wang, *Thermal design of multi-layered composite pipelines for deep water oil and gas production.* Int. Journal on Comput. Appl. Technology, 2012. **43**(3): p. 248-259.

10. Adeyanju, O. and L. Oyekunle, *Experimental study of wax deposition in a single phase sub-cooled oil pipelines.* University of Lagos. The Nigeria Annual International Conference and Exposition, Lagos, Nigeria, 2013.

11. Kirkpatrick, C.V., *Advances in Gas-lift Technology.* Drilling and Production Practice, American Petroleum Institute, 1959.

12. Ramey, H.J.J., *Wellbore Heat Transmission.* Society of Petroleum Engineers., 1962. **14**.

13. Willhite, G.P., *Over-all Heat Transfer Coefficients in Steam And Hot Water Injection Wells.* Journal of Petroleum Technology, 1967. **19**(5): p. 607 - 615.

14. Hasan, A.R., C.S. Kabir, and X. Wang, *Wellbore Two-Phase Flow and Heat Transfer During Transient Testing.* SPE Journal, 1998. **3**(02): p. 174 - 180.

15. Hasan, A.R., C.S. Kabir, and X. Wang, *Development and Application of a Wellbore/Reservoir Simulator for Testing Oil Wells.* SPE Formation Evaluation, 1997. **12**(3): p. 182-188.

16. Guo, B., S. Duan, and A. Ghalambor, *A Simple Model for Predicting Heat Loss and Temperature Profiles in Insulated Pipelines.* Society of Petroleum Engineers, 2006. **21**(1).

17. Guo, B., S. Duan, and A. Ghalambor, *A Simple Model for Predicting Heat Loss and Temperature Profiles in Thermal Injection Lines and Wellbores With Insulations.* Society of Petroleum Engineers. doi:10.2118/86983-MS, 2004.

18. Warming, R.F. and R.M. Beam, *Upwind second-order difference schemes and applications in unsteady aerodynamic flows.* 2nd Computational Fluid Dynamics Conference, 1975.

19. Mallick, P.K., *Fiber-Reinforced Composites: Materials, Manufacturing, and Design, Third Edition*. 2007: CRC Press

20. Hanna, Y., et al., *New Tendon and Riser Technologies Improve TLP Competitiveness in Ultra Deepwater.* Offshore Technology Conference. doi:10.4043/12963-MS, 2001.

21. Saad, P., M.M. Salama, and O. Jahnsen, *Application of Composites to Deepwater Top Tensioned Riser Systems.* ASME 2002 21st International Conference on Offshore Mechanics and Arctic Engineering, doi:10.1115/OMAE2002-28325, 2002.

22. Salama, M.M., D.B. Johnson, and J.R. Long, *Composite Production Riser Testing and Qualification.* Society of Petroleum Engineers. doi:10.2118/50971-PA, 1998.

23. Salama, M.M., et al., *The First Offshore Field Installation for a Composite Riser Joint.* Offshore Technology Conference. doi:10.4043/14018-MS, 2002.

24. Jones, R.M., *Mechanics of Composite Materials*. 1998: CRC Press.

25. Abdelpakey, M.H. and M.S. Shehata, *NullSpaceNet: Nullspace Convoluional Neural Network with Differentiable Loss Function.* arXiv:2004.12058, 2020.

26. Minsch, N., et al., *Analysis of Filament Winding Processes and Potential Equipment Technologies.* Procedia CIRP, 2017. **66**: p. 125-130.

27. Picard, D., et al., *Composite Carbon Thermoplastic Tubes for Deepwater Applications.* Offshore Technology Conference, https://doi.org/10.4043/19111-MS, 2007.

28. Kirchhoff, G., *Über das Gleichgewicht und die Bewegung einer elastischen Scheibe".* Reine und Angewante Mathematik (Crelle), 1850. **40**: p. 51-88.

29. Love, A., *A Treatise on the Mathematical Theory of Elasticity, 2nd Edition,*. Cambridge University Press, 1906.

30. Nakhla, S., *Lecture notes on solid mechanics and composite materials.* Memorial Universty, January 2016.

31. *MatWeb, searchable database of meterial properties.* http://www.matweb.com, last checked July 23rd 2019.

32. Gay, D., S.V. Hoa, and S.W. Tsai, *Composite Materials: Design and Applications*. 2002: CRC Press.

33. DaSilva, R.F., et al., *Optimization of composite catenary risers.* Marine Structures, 2013. **33**: p. 1-20.

34. Tong, R., *Cost Analysis on L-Shape Composite Component Manufacturing* 2012: The Department of Mechanical and Industrial Engineering, Concordia University.

APPENDIX A: Design Data for Composites

The data in this appendix is taken from [30].

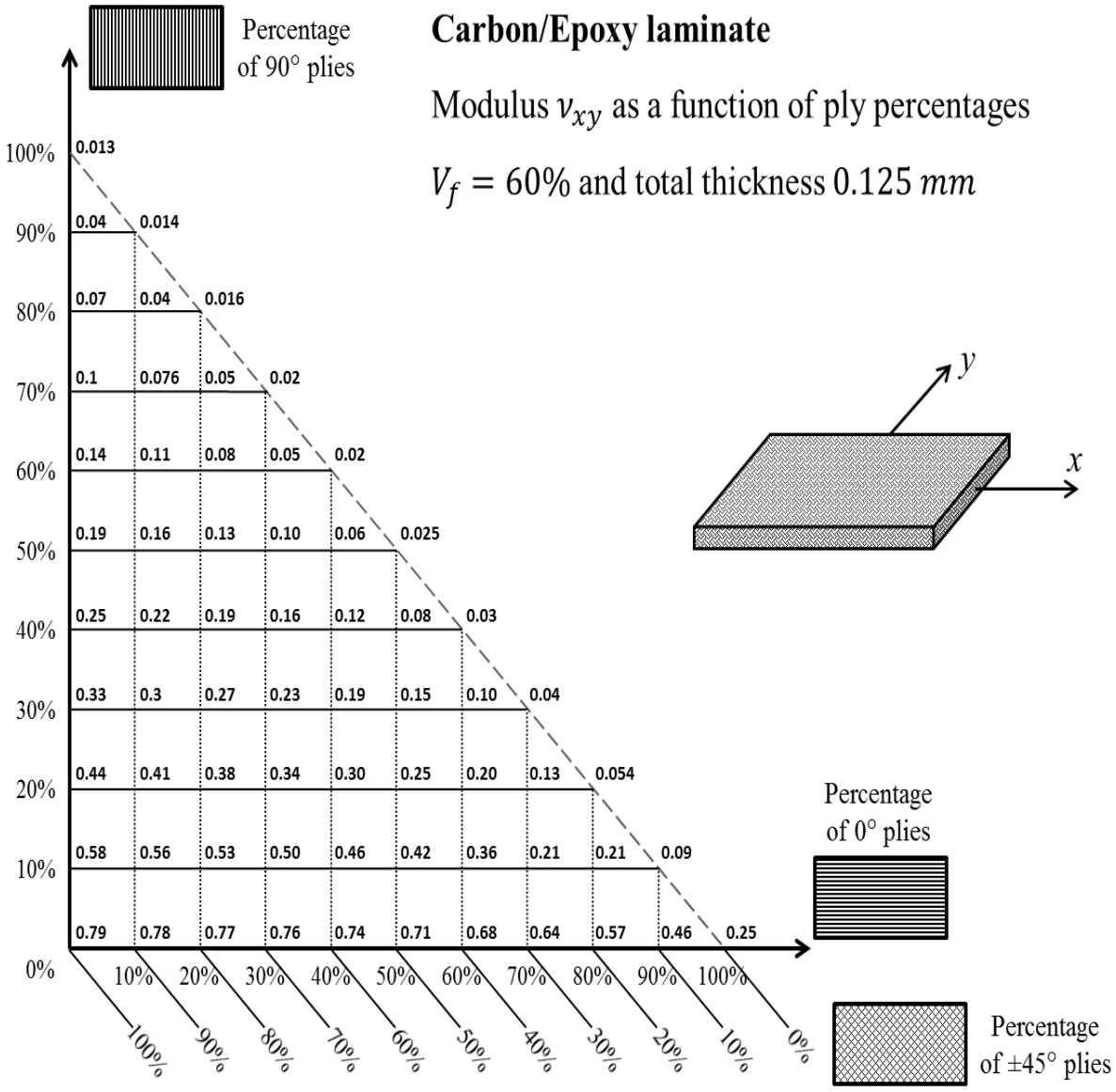

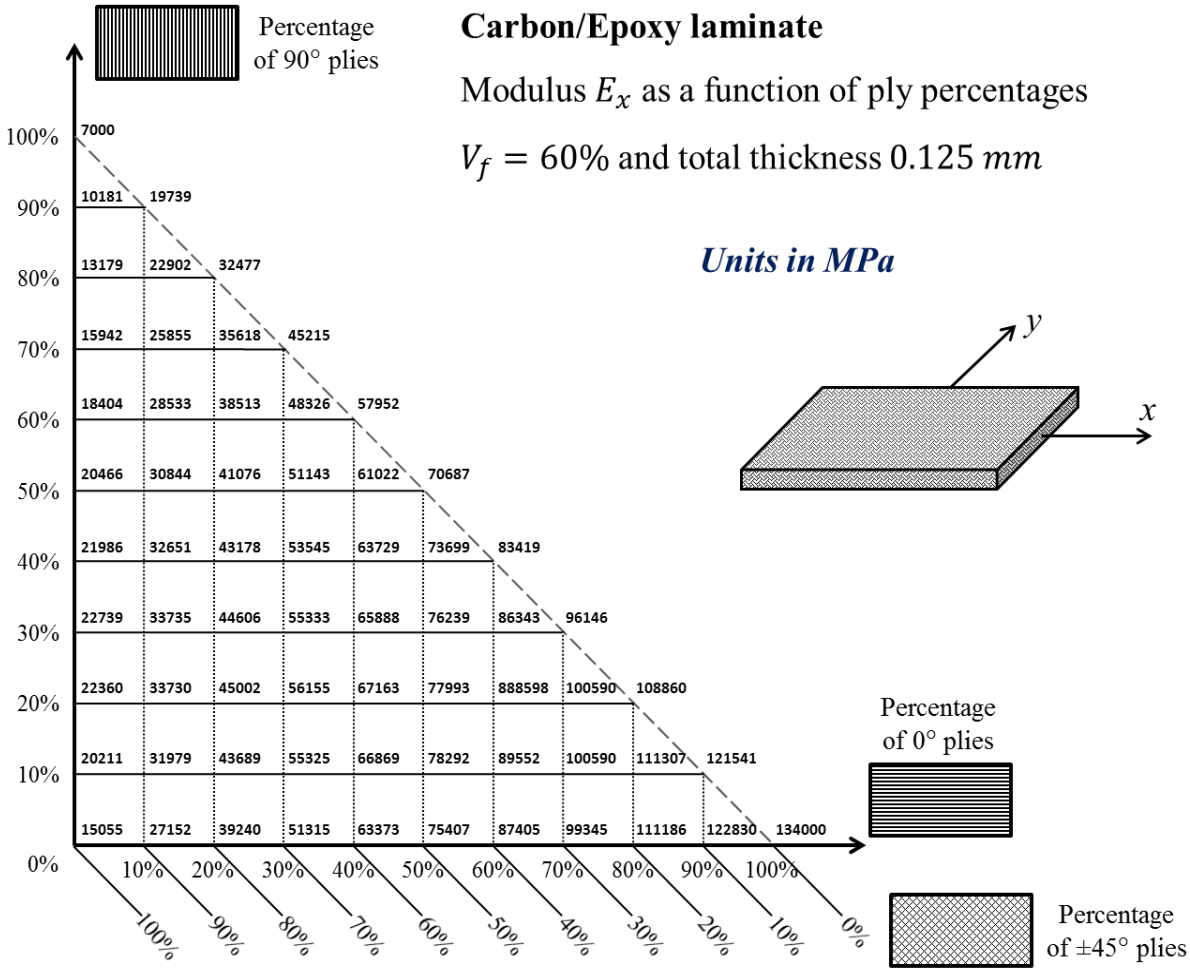
Carbon/Epoxy laminate
Modulus E_x as a function of ply percentages
$V_f = 60\%$ and total thickness $0.125\ mm$
Units in MPa
Percentage of 90° plies
Percentage of 0° plies
Percentage of ±45° plies
y
x
100%
90%
80%
70%
60%
50%
40%
30%
20%
10%
0%
7000
10181 19739
13179 22902 32477
15942 25855 35618 45215
18404 28533 38513 48326 57952
20466 30844 41076 51143 61022 70687
21986 32651 43178 53545 63729 73699 83419
22739 33735 44606 55333 65888 76239 86343 96146
22360 33730 45002 56155 67163 77993 888598 100590 108860
20211 31979 43689 55325 66869 78292 89552 100590 111307 121541
15055 27152 39240 51315 63373 75407 87405 99345 111186 122830 134000
10% 20% 30% 40% 50% 60% 70% 80% 90% 100%
100% 90% 80% 70% 60% 50% 40% 30% 20% 10% 0%

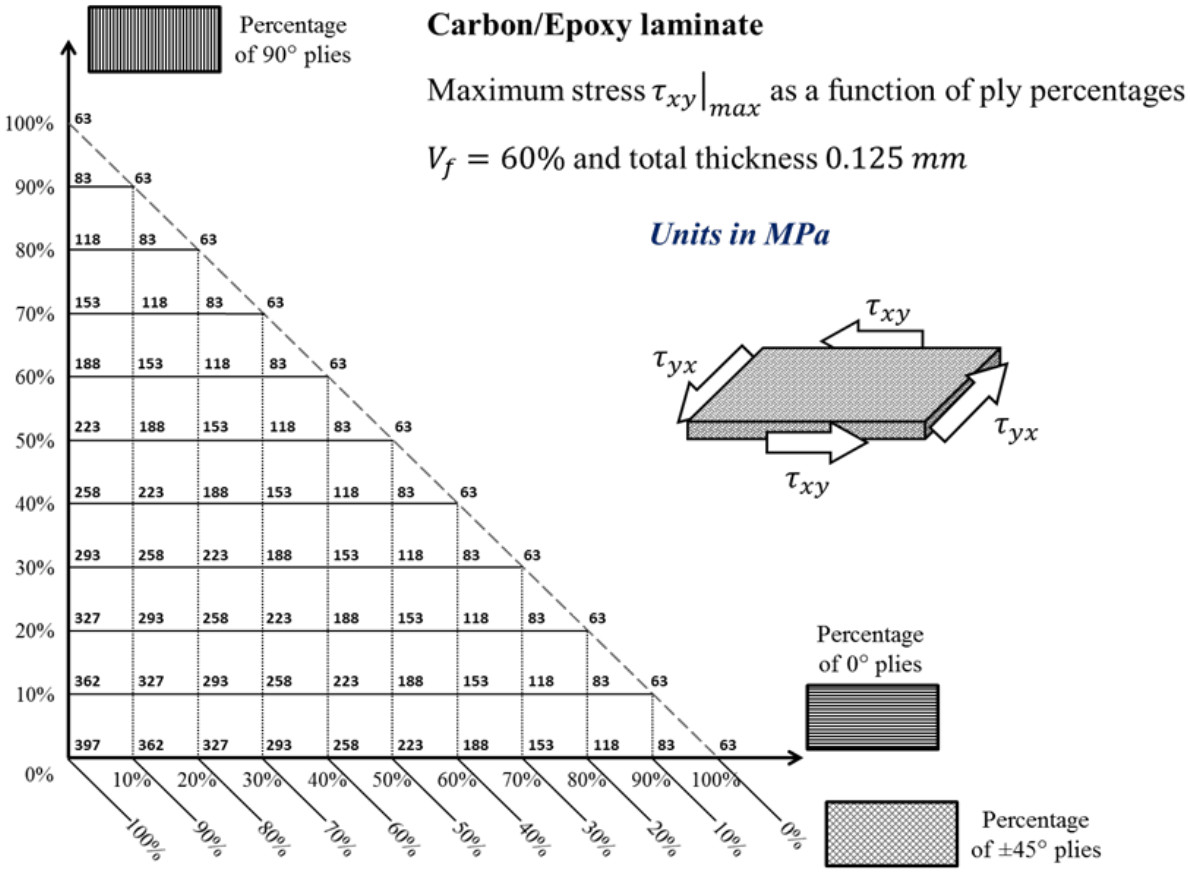
Carbon/Epoxy laminate
Maximum stress $\tau_{xy}|_{max}$ as a function of ply percentages
$V_f = 60\%$ and total thickness $0.125\ mm$
Units in MPa
Percentage of 90° plies
Percentage of 0° plies
Percentage of ±45° plies
τ_{xy}
τ_{yx}
τ_{yx}
τ_{xy}
100% 63
90% 83 63
80% 118 83 63
70% 153 118 83 63
60% 188 153 118 83 63
50% 223 188 153 118 83 63
40% 258 223 188 153 118 83 63
30% 293 258 223 188 153 118 83 63
20% 327 293 258 223 188 153 118 83 63
10% 362 327 293 258 223 188 153 118 83 63
0% 397 362 327 293 258 223 188 153 118 83 63
10% 20% 30% 40% 50% 60% 70% 80% 90% 100%
100% 90% 80% 70% 60% 50% 40% 30% 20% 10% 0%

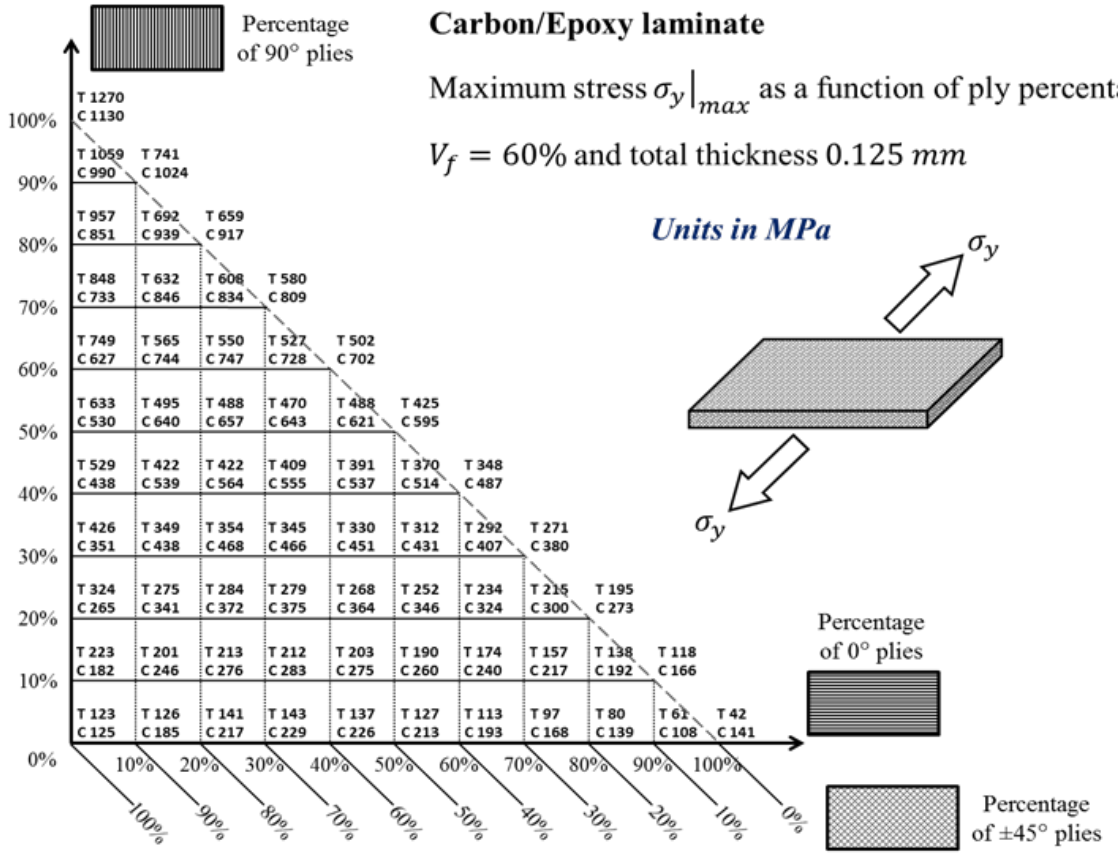
Carbon/Epoxy laminate
Maximum stress $\sigma_y|_{max}$ as a function of ply percentages
$V_f = 60\%$ and total thickness $0.125\ mm$
Units in MPa
Percentage of 90° plies
Percentage of 0° plies
Percentage of ±45° plies
σ_y
σ_y
100% T 1270 C 1130
90% T 1059 C 990 T 741 C 1024
80% T 957 C 851 T 692 C 939 T 659 C 917
70% T 848 C 733 T 632 C 846 T 608 C 834 T 580 C 809
60% T 749 C 627 T 565 C 744 T 550 C 747 T 527 C 728 T 502 C 702
50% T 633 C 530 T 495 C 640 T 488 C 657 T 470 C 643 T 488 C 621 T 425 C 595
40% T 529 C 438 T 422 C 539 T 422 C 564 T 409 C 555 T 391 C 537 T 370 C 514 T 348 C 487
30% T 426 C 351 T 349 C 438 T 354 C 468 T 345 C 466 T 330 C 451 T 312 C 431 T 292 C 407 T 271 C 380
20% T 324 C 265 T 275 C 341 T 284 C 372 T 279 C 375 T 268 C 364 T 252 C 346 T 234 C 324 T 215 C 300 T 195 C 273
10% T 223 C 182 T 201 C 246 T 213 C 276 T 212 C 283 T 203 C 275 T 190 C 260 T 174 C 240 T 157 C 217 T 138 C 192 T 118 C 166
0% T 123 C 125 T 126 C 185 T 141 C 217 T 143 C 229 T 137 C 226 T 127 C 213 T 113 C 193 T 97 C 168 T 80 C 139 T 61 C 108 T 42 C 141
10% 20% 30% 40% 50% 60% 70% 80% 90% 100%
100% 90% 80% 70% 60% 50% 40% 30% 20% 10% 0%